Hydrologic similarity: Dimensionless runoff indices across scales in a semi-arid catchment

Lawani Adjadi Mounirou, Roland Yonaba, Mahamadou Koïta, Jean-Emmanuel Paturel, Gil Mahe, Hamma Yacouba, Harouna Karambiri

Version of Record: https://www.sciencedirect.com/science/article/pii/S0140196321001567
Manuscript_c982d948a0f1624ae54877e4033c7c89

Hydrologic similarity: dimensionless runoff indices across scales in a semi-arid catchment

Lawani Adjadi Mounirou [a], Roland Yonaba [a, *], Mahamadou Koïta [a], Jean-Emmanuel Paturel [b], Gil Mahé [b], Hamma Yacouba [a], Harouna Karambiri [a]

[a] *International Institute for Water and Environmental Engineering (2iE), Laboratory of Water, HydroSystems and Agriculture (LEHSA), Rue de la Science 01 BP 594 Ouagadougou 01 Burkina Faso*

[b] *UMR 5569 HydroSciences Montpellier (HSM) - CC 57 - Université de Montpellier - 163, Rue Auguste Broussonnet - 34090 Montpellier*

*** Corresponding author:**

Roland YONABA

Laboratory of Water, HydroSystems and Agriculture (LEHSA)

International Institute of Water and Environmental Engineering (2iE)

Rue de la Science 01 BP 594 Ouagadougou 01 Burkina Faso

Phone : (00226) 76371116

Email : ousmane.yonaba@2ie-edu.org

ORCID : 0000-0002-3835-9559

Abstract

In this study, an assessment of similarity relationships in runoff measurements at different spatial scales was carried in a typical Sahelian landscape, under semi-arid climate in northern Burkina Faso (west African Sahel). The scales of observations considered are the plot scale (1 m², 50 m², 150 m²) and the sub-catchment scale (6.1 ha, 33.8 ha), under various soil surface conditions and slopes. These scales were monitored during six years (2010 to 2015) under natural rainfall. Based on monitoring data, a runoff potential index I_1 and an effective runoff index I_2 were developed, encapsulating the observation scale physical characteristics into dimensionless forms, hence reducing their sensitivity to the scale effects. These indices helped in assessing hydrological similarity across measurement scales. Results showed that runoff decreased with the increase of the observation scale size. Besides, dimensionless indices vary following a logarithmic decay relationship with the scale size ($R^2 > 0.98$). Such results highlight the non-linear nature of runoff processes and also promotes similarity analysis as a means to model hydrological processes using soil surface and landscape descriptors.

Keywords: Dimensional analysis; Hydrologic similarity; Runoff; Scale effect; Scaling law.

1. Introduction

The hydrologic similarity concept relates to the similarity in how catchments or surface units respond to rainfall. As a basis for catchment classification, this concept is helpful in transferring and generalizing knowledge in hydrology, but also in assessing the potential impacts of environmental change (Sawicz et al., 2011). Yet, hydrologists do not agree upon a consensus on catchment classification systems: in essence, the challenge lies in setting a classification framework integrating the spatial and temporal variability of hydrodynamic conditions which explicitly defines a catchment response, while accounting for uncertainty (Wagener et al., 2007).

A wide range of previous studies helped in gaining foundational insights at how hydrological processes are generated (Sivapalan and Kalma, 1995; Mayor et al., 2011; Mounirou et al., 2012; Mayerhofer et al., 2017). These studies contributed to a better characterization of runoff at the local scale. In most cases, the plots were installed on homogeneous units (in terms of soil surface conditions) in order to assess the typical runoff response of such soil surface conditions. Further research efforts built upon this knowledge and addressed the effect of scale on runoff. The dominant and consensual result often reported is that runoff decreases as the observation scale (or contributing area) increases (Kirkby et al., 2002; Gomi et al., 2008). Several root causes have been identified to support this observation. On agricultural areas, the scale effect on runoff has been related to a re-infiltration process (occurring at the downstream of the flow path), fostered by the spatial variation in soil permeability, during short duration and low-intensity rainfall events (Corradini et al., 1998; Jetten et al., 1999; Cerdan et al., 2004). Some studies also showed that the scale effect was mainly attributable to the rainfall intensity pattern (during an event), whereas the length and inclination of the soil surface slope amplify its effect (Stomph et al., 2002; Van de Giesen et al., 2005).

In arid and semi-arid areas, it was reported that the rainfall intensity and duration are the major factors explaining the scale effect (Reaney et al., 2007; Van de Giesen et al., 2011; Mohamadi and Kavian, 2015). However, in these environments, a significant link was identified between the runoff and the preponding rainfall (that is the minimal amount of rainfall depth after which the runoff process is triggered), hence contributing to the scale effect (Cammeraat, 2002, 2004; Boix-Fayos et al., 2007; Antoine et al., 2011; Cantón et al., 2011; Mayor et al., 2011; Miyata et al., 2019). In the recent years, the scale problem has been

the subject of much research, often prompted by the need to explain hydrologic behaviour at the catchment scale and therefore formulate answers to key challenges arising in water resource management. At the catchment level, the scale effect is mostly due to the emergence of specific elements such as ponds and infiltration wells, which are not perceptible at the plot scale because of the relative homogeneity at smaller scales (Lesschen et al., 2009; Mayor et al., 2011; Yonaba et al., 2021; Gbohoui et al., 2021). Another reported cause of the scale effect on runoff lies in the inherent non-linearity nature of the runoff process as it stems from complex relationships and transformations interacting altogether in the hydrological cycle (Sivapalan et al., 2002; Puech et al., 2003; Cerdan et al., 2004; Cantón et al., 2011). Overall, it appears that even though several identified causes can affect runoff, some factors are emergent given a specific scale but become overshadowed by others as the scale changes.

Thanks to the large collection of studies carried at the plot scale to understand and assess runoff mechanisms on different types of soil surface conditions and under various rainfall patterns, the dominant factors governing surface runoff processes have been well documented. However, the use of plots highlights the problem of representativeness as the investigated surface is limited. Moreover, the location of the plot is likely to influence the observations (Cammeraat, 2004; Mathys et al., 2005). It is therefore critical to assess the extent to which runoff observations across scales can be effectively linked together. An effective approach to this problem is the use of similarity parameters. This study aims to determine whether the mechanisms of surface runoff generation at different scales obey the same dimensionless relationships through the use of dimensionless variables. Such dimensionless numbers would then provide a basis to compare the respective contribution of different factors of runoff production across different spatial scales. Dimensional analysis helps define similarity relationships between different scales. It consists in reducing the number of dimensional variables describing a system to a smaller subset of dimensionless quantities, hence summarizes information from a given scale in the form of dimensionless numbers, related by a logical or an empirical relationship (Tillotson and Nielsen, 1984; Wagener et al., 2007; Peters-Lidard et al., 2017). Our focus on *scaling* and *similarity* directs attention to a challenging problem, yet unresolved, in the hydrologic sciences (Blöschl et al., 2019). We define *scale* as a "*characteristic length (or time) of process, observation, model*" whereas *scaling* is termed as the "*transfer of information across scales*". Also, we consider *similarity* to be present when the characteristics of a system can relate to those of another system through a scale factor (Peters-Lidard et al., 2017). Dimensional analysis offers an

interesting framework to shed some light in studying how runoff scales in space, as it offers to possibility to encapsulate and account for multiple characteristics of the observation scale (size, slope inclination, surface roughness, infiltration capacity, soil moisture) and as well as those of the rainfall (intensity, amount). Yet, to date, only a few developments and applications of this approach have been investigated in hydrology. Sivapalan et al. (1987), among the first, used similarity analysis to characterise surface runoff processes. Julien and Moglen (1990) analysed runoff through a dimensionless index based on the relationship between the rainfall duration and the equilibrium time. Likewise, Larsen et al. (1994) explained the variability of the runoff coefficient through a dimensionless index based on the rainfall intensity and the soil characteristics. Yet, further investigations are needed to expand the actual knowledge and possibly, to account for more factors affecting runoff generation.

The catchment of Tougou (37 km²), located in the Sahelian zone of Burkina Faso, in the West African Sahel, was chosen for this research. As a physical unit, the catchment of Tougou has been a field support site for a large number of studies targeting Sahelian landscapes and semi-arid climate and for more than 5 decades. The soil surface conditions found in the catchment landscape were found to be representative of the Sahelian strip, hence suitable to provide interesting insights regarding the runoff generation processes. Moreover, previous research work showed that surface runoff generation mechanisms in Tougou catchment exhibit similar characteristics as those observed in typical Sahelian hydrosystems (Albergel, 1987), especially regarding the dependence on soil surface conditions (Karambiri et al., 2003; Mounirou et al., 2012; Zouré et al., 2019; Mounirou et al., 2020; Yonaba et al., 2021). The objectives of this study are: (i) to analyse the hydrologic similarity of runoff in a catchment under a semiarid climate at different small spatial scales, ranging from the plot scale (1 m²) to sub-catchment scale (tens of hectares); (ii) to develop analytical relationships between dimensionless variables defining the hydrological functioning across different scales of observations.

2. Material and methods

2.1. Study area

The catchment of Tougou (37 km²) is located in the northern part of Burkina Faso, in the West African Sahel (**Fig. 1a**). The catchment is located within the Northern region of the country, more precisely in the Yatenga province. Its outlet is located at 13° 40' 56" N and 2° 13' 39" E geographical coordinates. The landscape features two dominants units of land use, which are cultivated soils estimated at 65% of the catchment area and degraded and

uncultivated soils covering 35% of the catchment area (Yonaba et al., 2021). Vegetation on the catchment is sparse and mostly made of savannah shrubs. According to the national soil survey database (IGB, 2002), three types of soil can be found within the area: (i) slightly evolved soils (covering 25% of the catchment), developing a sandy or sandy-gravel texture at the surface; (ii) mineral soils (covering 35% of the catchment) which tend to physical degradation, called '*zipelle'* by the local populations (Sawadogo et al., 2008); (iii) hydromorphic soils (covering 40% of the catchment) located in alluvial terraces and are mostly clayey, often highly silted (IGB, 2002).

The climate is characterized by a unimodal rainfall regime with a rainy season from June to October and a dry season from November to May. The rainfall in the Tougou catchment, as in the Sahelian region, is produced by the so-called "*Mesoscale Convective systems*" (MCSs), which are of large spatial extension and propagates from East to West. In the region, MCSs produce 80% of the annual rainfall, whereas the remaining 20% result from more localized storm systems (Mathon et al., 2002). The annual rainfall varies between 400 and 750 mm, with an annual average of 650 mm, whereas annual evapotranspiration is 2090 mm on average (Zouré et al., 2019).

As in most Sahelian landscapes, runoff processes are Hortonian due to the development of crusts at the soil surface, sealing the soil surface, limiting infiltration and favouring runoff (Casenave and Valentin, 1992). Also, rainfall intensities in the context are high, as their values range from 130 to 180 mm/h in 5 minutes and 70 to 90 mm/h in 30 minutes (Mounirou et al., 2012, 2020).

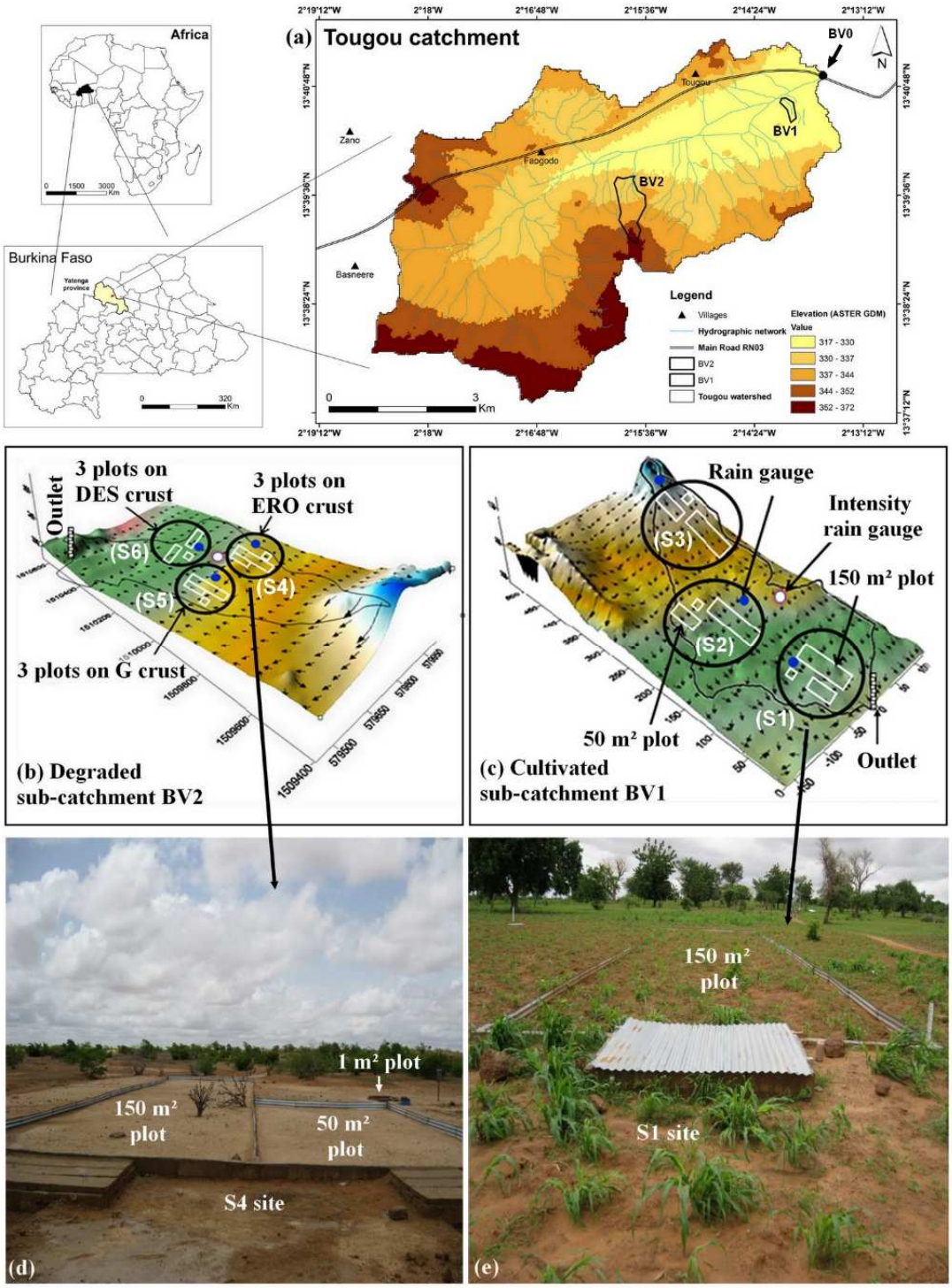

Fig. 1. Study area location and experimental design. (a) Localization of the catchment of Tougou. The sub-catchments locations BV_1 (cultivated) and BV_2 (degraded) are shown with black contour lines. Elevation on the entire catchment is derived from ASTER GDEM Digital Elevation Model, 30m resolution, tile N13W003, acquired from USGS EarthExplorer (https://gdemdl.aster.jspacesystems.or.jp/index_en.html). (b) Detailed view of the experimental layout in BV_2 (degraded sub-catchment). (c) Detailed view of the experimental layout in BV_1 (cultivated sub-catchment). (d) Field photograph of the experimental design at S4 site in the degraded sub-catchment (BV_2). (e) Field photograph of the experimental design at S1 site in the cultivated sub-catchment (BV_1).

144 **2.2. Experimental setup**

145 Two hydrologic units (sub-catchments) were selected in the catchment. These units are
146 homogeneous in terms of land use and soil surface conditions and are respectively identified
147 as cultivated (BV_1, 6.1 ha, **Fig. 1a, c**) and degraded/uncultivated (BV_2, 33.8 ha, **Fig. 1a, b**)
148 sub-catchments. Degraded and uncultivated refers to naturally occurring and undisturbed
149 soils, corresponding to barren and degraded land use/land cover (Anderson et al., 1976) and
150 developing a very low vegetation cover, mostly consisting of shrubs and herbaceous
151 (Mounirou, 2012). In each sub-catchment, three sites were selected for their homogeneity in
152 terms of soil type, land use and cropping systems. At each site, three plots with different sizes
153 (1, 50 and 150 m²) were installed (**Fig. 1d, e**). The plots locations were chosen on the field
154 where soil surface conditions could be assumed homogeneous, with identical agricultural
155 practices. However, the microrelief (in terms of roughness and surface storage capacity)
156 varied from one plot to another. Topographic surveys were conducted using a Trimble S6
157 total station, at various square mesh sizes: 50 cm on the plots of 50 m² and 150 m², 20 cm at
158 plot scale of 1 m²; 25 m² at the scale of the two sub-catchments (BV_1 and BV_2). These
159 topographic surveys helped in evaluating the average longitudinal slope of each plot and of
160 the sub-catchments: 6 measurements were made on 1 m² plots, 11 measurements on 50 m²
161 plots and 13 measurements on 150 m² plots. The detailed description of the soil surface
162 conditions on all plots is given in **Table 1**.

163 The soil types and their measured physical properties are further described in **Table 2**. The
164 soil texture was determined through soil sieving and sedimentation protocol
165 (AFNOR/NFISO11277) applied to 9 soil samples per site. Saturated hydraulic conductivity
166 K_S was measured with the double-ring infiltrometer (Reynolds and Topp, 2008). Bulk density
167 ρ_b was estimated from undisturbed soil samples through the core method after oven drying at
168 105°C for 48h (Jawuoro et al., 2017) and calculated according to **Equation 1**:

$$\rho_b = m_s/V \quad (1)$$

169 where m_s (g) is the mass of the dry weight of soil (g) and V (cm^3) is the soil volume. Porosity
170 p was then derived from the bulk density values ρ_b, according to **Equation 2** (Jawuoro et al.,
171 2017):

$$p = 1 - \rho_b/\rho_s \quad (2)$$

where ρ_b is the bulk density, ρ_s is the particle density taken as 2.65 g.cm^{-3} (Mounirou, 2012; Jawuoro et al., 2017). The Manning roughness (n) values were determined according to the median grain diameter d_{50} of the soil at each site, based on Strickler's formula, as given by **Equation 3** (Chanson, 2004):

$$\frac{1}{n} = 21.1\, d_{50}^{-1/6} \tag{3}$$

where $n\ (s.m^{-1/3})$ is the Manning roughness coefficient and $d_{50}\ (m)$ is the median grain diameter size in a soil sample distribution.

Table 1.
Detailed description of soil surface conditions on all the plots in the experimental setup.

Site name	Unit name	Hydrological unit type	Size	Average slope (%)	Soil surface condition	Land use
Site S_1	S_1-1	Plot	1 m² (1x1)	1.60 ± 0.43	C	Cultivated
	S_1-50	Plot	50 m² (5x10)	1.80 ± 0.14		
	S_1-150	Plot	150 m² (6x25)	1.35 ± 0.15		
Site S_2	S_2-1	Plot	1 m² (1x1)	1.70 ± 0.50		
	S_2-50	Plot	50 m² (5x10)	1.40 ± 0.19		
	S_2-150	Plot	150 m² (6x25)	1.60 ± 0.10		
Site S_3	S_3-1	Plot	1 m² (1x1)	4.00 ± 0.52		
	S_3-50	Plot	50 m² (5x10)	4.20 ± 0.59		
	S_3-150	Plot	150 m² (6x25)	2.85 ± 0.15		
Site S_4	S_4-1	Plot	1 m² (1x1)	0.75 ± 0.16	ERO	Degraded and uncultivated
	S_4-50	Plot	50 m² (5x10)	1.25 + ± 0.09		
	S_4-150	Plot	150 m² (6x25)	0.93 ± 0.08		
Site S_5	S_5-1	Plot	1 m² (1x1)	0.90 ± 0.31	G	
	S_5-50	Plot	50 m² (5x10)	0.96 ± 0.11		
	S_5-150	Plot	150 m² (6x25)	0.80 ± 0.14		
Site S_6	S_6-1	Plot	1 m² (1x1)	2.30 ± 0.24	DES	
	S_6-50_1	Plot	50 m² (5x10)	2.10 ± 0.28		
	S_6-50_2	Plot	150 m² (5x10)	3.55 ± 0.32		
	BV1	Sub-catchment	6.1 ha	1.91 ± 0.28	C	Cultivated
	BV2	Sub-catchment	33.8 ha	1.18 ± 0.16	ERO, G, DES	Degraded and uncultivated
	BV0	Catchment	37 km²	0.60 ± 0.11	C, ERO, G, DES	Heterogeneous

In the size column, for each unit at each site, the plot dimensions are given in parenthesis, using the following convention: (*l x L*), where l and L stands respectively for the plot width and length, both in meters. The plot length *L* is also the runoff length. Soil surface condition uses the naming convention for surface feature crusts presented in Casenave and Valentin (1992): erosion crust (ERO), desiccation crust (DES), agricultural crust (C) and gravel pavement crust (G). Regarding slope determination, 6 measurements were made on 1 m² plots, 11 measurements on 50 m² plots and 13 measurements on 150 m² plots. The term "*crust*" designates a thin and stratified layer developing at the soil surface, which has undergone changes under the effect of meteorological, faunal or anthropogenic factors. Type C crusts are made of one or two micro-horizons, generally forming on clayey or sandy soils. ERO crusts are made of a single and thin micro-horizon, harden, clayey, prone to crackling when drying up. DES crusts are made of a single sandy micro-horizon, very fragile. G crusts are made of a single micro-horizon containing coarse sediments (diameter > 2 mm).

Table 2.
Soil type and physical properties at monitoring sites.

Site	Soil type	Tillage operations	Crop type	K_S (mm.h^{-1})	K_S (mm.h^{-1}) (Casenave and Valentin, 1992)	Bulk Density ρ_b (g.cm^{-3})	Porosity p (%)	Manning n (s.m$^{-1/3}$) roughness
S1	Loam	Row sowing + ploughing + weeding + hoeing	Millet, sorghum and cowpea	21 – 25	15 - 35	1.40 – 1.46	45 – 47	0.050
S2	Sandy	Row sowing + ploughing + ridging	Millet, sorghum and cowpea	27 – 33		1.36 – 1.44	46 – 49	0.060
S3	Sandy gravelly	Row sowing + weeding + hoeing	Millet, sorghum and peanut	16 – 19		1.46 – 1.48	44 – 45	0.065
S4	Dry clay	No tillage	No cropping	2 – 2.5	2 – 4	1.58 – 1.61	39 – 40	0.015
S5	Gravelly			3 – 3.5	3 – 5	1.88 – 1.94	27 – 29	0.020
S6	Sand			12 – 15	10 – 20	1.66 – 1.70	36 – 37	0.025

K_S refers to the soil saturated hydraulic conductivity. Number of infiltration measurements by site: 12. Number of porosity measurements by site: 9.

The values in **Table 2** are in line with the observations made on similar types of crust in the Sahelian region reported by (Casenave and Valentin, 1992) and they also reflect the range of variability for each parameter, especially for the soil hydrodynamic properties in cultivated areas. However, within the same site, this range of variability is lesser and therefore, the hydrodynamic properties of the soil at each site are assumed homogeneous, and cultivation practices identical. On each site, only the microrelief (slope, surface roughness and surface storage capacity) is considered to be varying from one plot to another. Furthermore, the analysis of bulk density and porosity values (**Table 2**) in the first 15 cm of the soils of the plots showed that the soil is more compact on bare and degraded areas than on cultivated areas.

In the Tougou catchment, the major tillage operations carried on cultivated soils are ploughing, followed by sowing or manual weeding (weeding associated to hoeing) or weeding with animal traction (Marchal, 1983; Barbier et al., 2009; Zouré, 2019). These operations break the crusts developing at the soil surface and therefore improves infiltration. Partitioned ridging is also practised in Tougou catchment and also helps in reducing runoff and promote infiltration (Nyamekye et al., 2018; Zouré, 2019). The sizing and description of the tillage operations carried in Tougou catchment is presented in **Table 3**. It is also

interesting to note that stone bunds are heavily used in association with these tillage operations, mostly as a soil conservation measure (Nyamekye et al., 2018; Zouré, 2019).

Table 3.
Sizing and description of tillage operation carried on cultivated fields in Tougou catchment (Dugué et al., 1994).

Ridge spacing/density	Tillage operations
Millet : 80 cm x 80 cm Sorghum: 80 cm x 40 cm Groundnut: 40 cm x 20 cm Cowpea: 80 cm x 40 cm	ploughing (0 – 15 cm depth), weeding (0-5 cm depth), hoeing (0 - 5 cm depth), ridging (15 – 20 cm)

The tillage operations described in this table are often combined by farmers in Tougou catchment (Barbier et al., 2009).

2.3. Surface runoff and rainfall monitoring

Each plot of 1 m² was isolated by a metal sheet frame, buried into the ground at a depth of 10 cm. The plot was also equipped with an outlet connected to a PVC pipe leading runoff to a buried tank for runoff collection and measurement. Plots of 50 and 150 m² were isolated from outside overland flow run-on using metallic sheet frames also buried at 10 cm depth into the ground; downstream, the plots were equipped with a collector composed of a concrete tank (with 2 or 3 compartments respectively for plots of 50 and 150 m²). Level gauges were installed in each tank to monitor runoff depths.

Rainfall events were monitored from 2010 to 2015 (6 years), during each rainy season, using a network of 12 rain gauges, including 6 rain gauges installed on runoff monitoring sites (one per each site), whereas the remaining 6 were spread throughout the catchment to assess the spatial variability of rainfall. Also, 5 tipping bucket rain gauges (including 1 per sub-catchment, and the remaining 3 spread throughout the catchment) were used for rainfall intensity measurement at 5 minutes timesteps. Average rainfall amount per event was evaluated using Thiessen averaging method.

At the outlets of the sub-catchments BV_1 and BV_2 and the entire catchment named BV_0, a control section equipped with an *OTT Thalimedes* water level logger. Further, recorded water levels were converted to series of instantaneous discharges using rating curves for each control section. These rating curves were developed through a simple power-law equation fit to direct measurements at the outlet of each control section. Derived hydrographs were converted to runoff volumes and further, runoff depths for all the recorded rainfall events. Runoff monitoring was also carried out during six years, from 2010 to 2015.

2.4. Runoff dimensionless indices

In this study, dimensionless numbers were developed to reduce the effect of the size of the observation scale on runoff.

The dimensionless indices proposed in this study were developed considering the topography, surface roughness, saturated hydraulic conductivity, rainfall amount and intensity. The theoretical basis and mathematical development leading to the expression of these dimensionless indices is further detailed and discussed in **Appendix A**. The proposed indices are the following:

(i) the *runoff potential* dimensionless index (I_1) expressed as the ratio of the plot runoff coefficient to the square root of its slope. As defined in **Equation 4**, it expresses the runoff potential of the plot and reduces the effect of the slope (explicitly slope) on runoff production. This formulation results from a physically-based modelling of runoff based on Manning flow formula (Manning, 1891; Chanson, 2004).

$$I_1 = \frac{K_r}{\sqrt{S_0}} \tag{4}$$

where K_r is the runoff coefficient of the plot and S_0 is the slope of the plot. Runoff coefficients were evaluated on an event scale basis, as a ratio of the observed runoff to the rainfall.

(ii) the *effective runoff* dimensionless index (I_2), expressed as the ratio of the runoff depth (R) measured at a given observation scale, out of the term ($P - Ks \times Te$), as shown in **Equation 5**:

$$I_2 = \frac{R}{P - K_s \times T_e} \tag{5}$$

where *R (mm)* is the runoff depth, *P (mm)* is the rainfall amount, *Ks* ($mm.h^{-1}$) is the saturated hydraulic conductivity and *Te (h)* the time to equilibrium state, i.e., the time to the establishment of a steady-state runoff.

Te is also referred to as the *kinematic time to equilibrium* (Julien and Moglen, 1990) and is given by **Equation 6**:

$$T_e = \beta \left(\frac{L}{\alpha \times i^{\beta-1}} \right)^{\frac{1}{\beta}} \tag{6}$$

where $L\ (m)$ is the plot length, i is the infiltration excess, α and β are parameters. Combining Manning resistance turbulent flow equation with a kinematic wave approximation yields $\beta = 5/3$ (Julien and Moglen, 1990). Parameter α, on the other hand, is given by **Equation 7**:

$$\alpha = \frac{1}{n} \times \sqrt{S_0} \tag{7}$$

where S_0 is the plot slope and $n\ [s.m^{-1/3}]$ is the Manning roughness coefficient. The product term ($Ks\ x\ Te$) in the dimensionless number I_2 (**Equation 5**) expresses infiltration losses occurring along the flow path on the plot. Removing this term from the rainfall input confers to the dimensionless number I_2 the ability to reduce the scale effect due to re-infiltration downstream of the plot.

At the sub-catchment scale, the evaluation of T_e requires an estimation of surface runoff velocities $V_p\ (m.s^{-1})$ on the measurement plots and $V_h\ (m.s^{-1})$ in the sub-catchment and catchment drainage system. The geometry of the drainage system was assumed to be invariant over time and velocities uniform at each observation scale. Besides, to reduce the number of parameters, we relied on the previous research work of which estimated that runoff velocity in drainage network (V_h) is approximately ten (10) times higher than the runoff velocity at the plot scale (V_p) (Gresillon and Taha, 1998; Tatard et al., 2008). As such, a constant ratio between these velocities was defined as given in **Equation 8**:

$$V_h = 10V_p\ , \quad V_p = \frac{L}{T_e} \tag{8}$$

3. Results

3.1. Rainfall characteristics

Table 4 shows the daily rainfall distributions statistics from 2010 to 2015. Maximum daily rainfall amount ranges between 41.8 and 114 mm during the entire observation period, whereas cumulative annual rainfall varied between 450 and 730 mm. The interquartile range (IQR), median (Q2) and mean daily rainfall events are also presented and illustrates the skewness of the distributions towards smaller daily rainfall values.

Table 4.
Daily rainfall distribution statistics in Tougou catchment from 2010 to 2015.

Annual rainfall events	2010	2011	2012	2013	2014	2015
Annual rainfall (mm)	671.6	449.3	697.7	578.6	624.3	729.6
Number of events	39	30	35	38	30	34
Daily minimum rainfall (mm)	1.6	1.6	2.2	2.8	4.7	3.7
Q1 (first quartile) (mm)	7.0	5.8	7.4	8.4	12.2	7.8
Q2 (median) (mm)	18.1	10.7	13.8	13.7	19.4	14.0
Mean (mm)	17.2	15.0	19.9	15.2	20.8	21.5
Q3 (third quartile)	24.4	23.4	29.6	20.9	26.8	24.6
Daily maximum rainfall (mm)	53.5	53.9	81.6	41.8	47.4	114.0

The monthly rainfall amount and rainfall intensities statistics are presented in **Table 5**. No significant correlation was found between the rainfall amount and its duration, highlighting the high variability in the rainfall intensity across the rainfall events. Maximum rainfall intensities recorded peaked at 120 $mm.h^{-1}$ in 5 minutes (*Imax-5mn*) and 70 $mm.h^{-1}$ in 30 minutes (*Imax-30mn*). In terms of rainfall amount, during the six years of monitoring, nine (09) daily events exceeded 50 mm in amount, the most important one being the event which occurred on 05/08/2015, which peaked at 114 mm.

Table 5.
Monthly rainfall statistics in Tougou catchment from 2010 to 2015.

Months	Rainfall amount					Rainfall intensity			
	Pd (mm)		Pm (mm)		Annual rainfall percent	Imax-5mn ($mm.h^{-1}$)		Imax-30mn ($mm.h^{-1}$)	
	Avg	σ	Avg	σ		Avg	σ	Avg	σ
June	41.6	10.8	101.8	35.2	16%	81.6	7.5	42.2	6.2
July	43.3	12.1	146.5	42.7	23%	82.5	10.9	42.8	8.5
August	57.8	32.8	218.0	43.0	35%	95.9	16.7	58.8	9.4
September	35.9	16.6	119.6	41.8	19%	78.5	29.0	42.7	12.5
October	21.6	9.6	41.5	26.3	7%	37.6	14.9	26.7	11.5

Pd: average maximum daily rainfall. Pm: cumulative average monthly rainfall. Avg: average. σ: standard deviation. Imax-5mn: maximum rainfall rate in 5 minutes. Imax-30mn: maximum rainfall rate in 30 minutes.

It was also observed that in general, all rainfall events are homogeneous most of the time over the catchment, similarly to the findings reported in Mounirou (2012), Zouré (2019).

Examination of **Fig. 2** shows that, on average, nearly 32% of the rainfall events (corresponding to 10% of the annual rainfall volume) fall below 8.5 mm. The threshold of 8.5 mm was found to be the preponding rainfall value of the entire catchment in Mounirou (2012). **Fig. 2** shows that nearly 35% of the events, the highest share, fall between 10 and 20

mm and contributes to 27% on average of the annual rainfall volume. Also, 31.9% of the observed rainfall events are below 8.5 mm (the preponding rainfall) and accounts for 10% of the annual rainfall volume. Likewise, events above 40 mm account for 7.5% of the observed events, yet they generate nearly 27% of the annual rainfall volume.

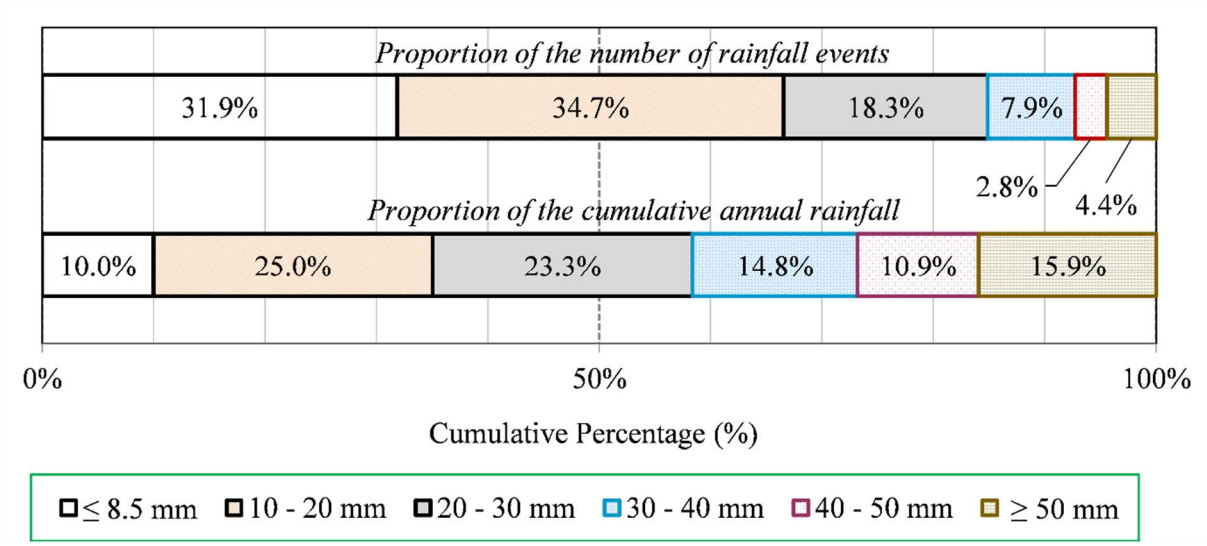

Fig. 2. Proportion of rainfall events per class. The upper bar chart shows the rainfall events distribution in terms of number of events. The lower bar chart shows the proportion of rainfall events in terms of annual rainfall volume. It can be seen that, for example, 31.9% of the rainfall events observed fall below 8.5 mm and account for 10% of the annual rainfall volume on average. Similarly, rainfall events above 40 mm are observed 7.5% of the time, but they generate nearly 27% of the annual rainfall volume.

3.2. Variability of annual surface runoff coefficients

Annual runoff coefficients values calculated on plots of 1, 50 and 150 m², hydrologic units (sub-catchments) of 6.1 ha and 33.8 ha and the catchment area of 37 km² are presented in **Fig. 3**.

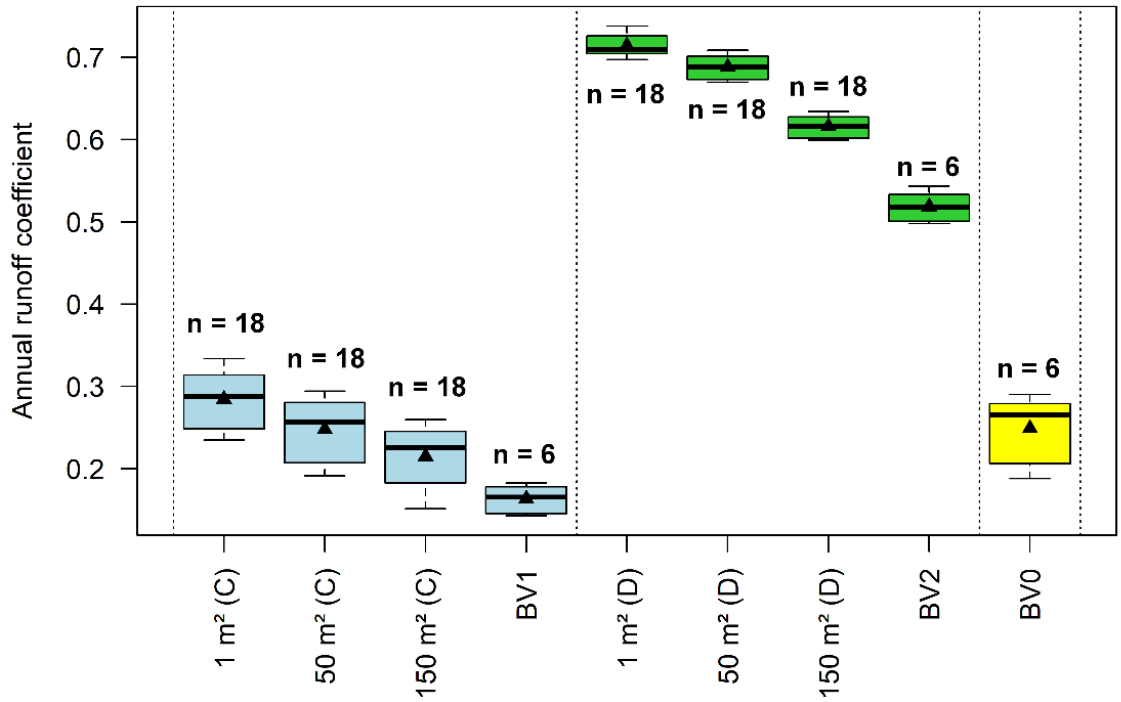

319

320 **Fig. 3.** Annual runoff coefficient distribution across the monitoring sites during 2010-2015. The suffix (C) stands
321 for plots on the cultivated sub-catchment BV1, whereas (D) stands for the degraded sub-catchment. BV_1 and
322 BV_2 refer to the runoff coefficients for the cultivated and degraded sub-catchments respectively. BV0 refers to
323 runoff coefficients observed for the entire catchment. The middle bar in the boxplots shows the median (Q2) of
324 the distribution, whereas the black triangle dot inside the boxplots shows the mean. The size of the distribution is
325 indicated above (or below) each boxplot.

326 The median (Q2) values of annual runoff coefficients associated with the interquartile range
327 (IQR) are as follows: on agricultural soils, runoff coefficients varied between 0.29 (0.25 -
328 0.31) (plot of 1 m²) to 0.23 (IQR: 0.19 – 0.24) (plot of 150 m²), whereas the average runoff
329 coefficient for the agricultural sub-catchment BV_1 (6.1 ha) was 0.17 (IQR: 0.15 – 0.18).
330 These values were significantly lower (**Table 6**) than those measured on degraded plots,
331 which went from 0.71 (IQR: 0.70 – 0.72) (plot of 1 m²) to 0.62 (IQR: 0.60 – 0.63) (plot of
332 150 m²), with the degraded and uncultivated catchment BV_2 (33.8 ha) presenting a median
333 annual runoff coefficient of 0.52 (IQR: 0.50 – 0.53).

Table 6.
Statistical comparison of runoff coefficients at different scales.

Comparison	t-Student p-value
1 m² plots (cultivated) - 1 m² plots (degraded and uncultivated)	**$0.31.10^{-6}$**
50 m² plots (cultivated) - 50 m² plots (degraded and uncultivated)	**$0.35.10^{-6}$**
150 m² plots (cultivated) - 150 m² plots (degraded and uncultivated)	**$0.56.10^{-6}$**
BV_1 (cultivated sub-catchment) – BV_2 (degraded and uncultivated sub-catchment)	**$0.10.10^{-9}$**
BV0 (catchment) – BV_1 (cultivated sub-catchment)	**0.004**
BV0 (catchment) – BV_2 (degraded and uncultivated sub-catchment)	**$7.50.10^{-6}$**

Significant values (at level $\alpha = 5\%$) are shown in bold. The comparison is made on runoff coefficient values calculated for all events observed during the monitoring period (2010-2015).

At all scales, degraded and uncultivated soils show a higher runoff production potential on average than cultivated soils under similar rainfall conditions. This can be explained by their higher compaction and crust development at the soil surface, which is limiting infiltration and favouring runoff. The entire catchment (37 km²) showed a median runoff coefficient of 0.27 (IQR: 0.22 – 0.28), which was above the median for the cultivated sub-catchment BV_1 and significantly smaller than the median for the degraded and uncultivated catchment BV_2. Such results can partly be explained by the heterogeneity and the hydrologic connectivity in terms of soil surface conditions in the catchment. However, the dominance of agricultural areas (65% of the catchment area) causes a global runoff coefficient on average which tends to the one observed on the corresponding sub-catchment BV_1.

It also appears that considering both cultivated or degraded and uncultivated soils, the runoff coefficients decrease as the scale increases. This observed decrease in runoff can be explained by several factors affecting runoff, such as the non-linearity nature of the runoff process (Sivapalan et al., 2002; Cerdan et al., 2010; Cantón et al., 2011), the spatial variability of soil infiltration (Cerdan et al., 2004; Mounirou et al., 2012; Miyata et al., 2019) but also the temporal pattern of rainfall (Stomph et al., 2002; Van de Giesen et al., 2005; Cristiano et al., 2019).On cultivated soils, coefficients of variation of runoff coefficient were respectively 14.17%, 16.87%, 19.46% and 10.25% at plots of 1 m², 50 m², 150 m² and the cultivated sub-catchment BV_1 (6.1 ha). These values were higher than those of degraded and uncultivated soils, which were respectively 2.12% (plot of 1 m²), 2.41% (plot of 50 m²), 2.41% (plot of 150 m²) and 3.54% (BV_2, 33.8 ha).

To further assess the influence of agricultural practices on the observed runoff coefficients through the change in soil surface conditions, the cumulative runoff evolution is plotted

against the cumulative rainfall. **Fig. 4** shows a typical example of such plot for the year 2010, on a cultivated plot of 150 m² at site S_2.

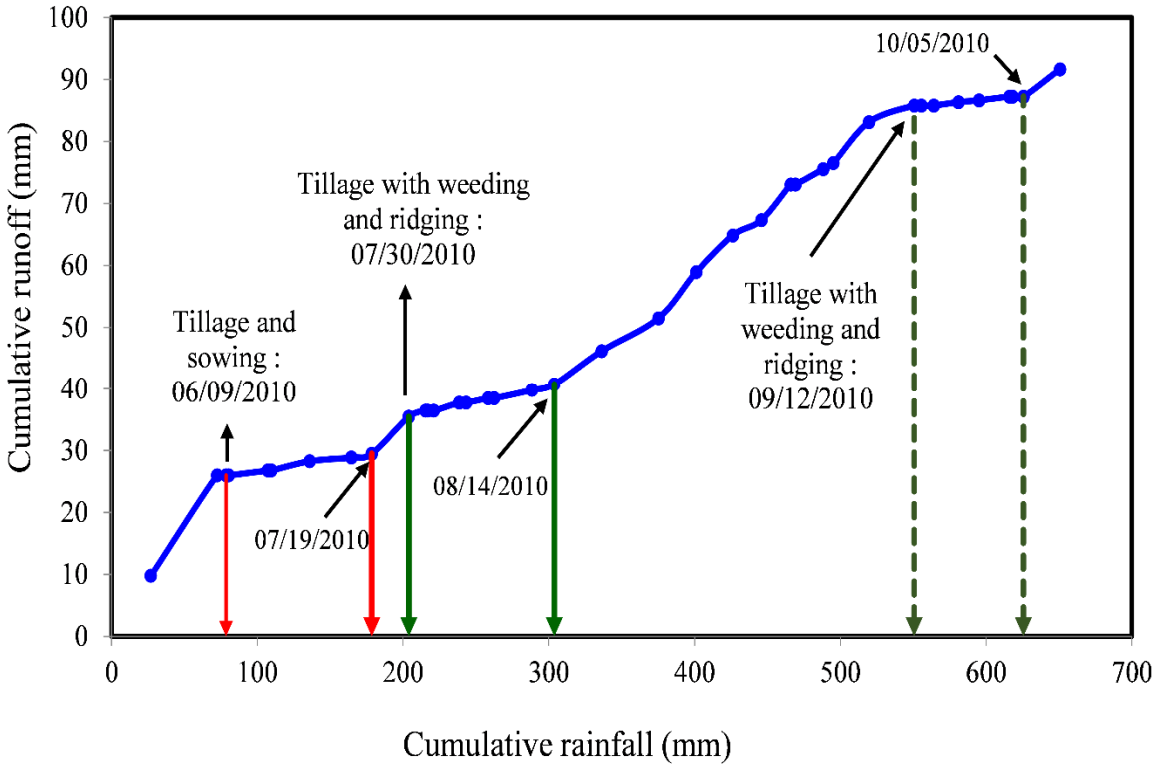

Fig. 4. Impact of soil management operations on the rainfall-runoff relationship. Data of 2010 year were used for this example. Tillage operation is carried in general three times during a rainy season. At its beginning (early June), tillage and sowing are carried on cultivated fields. Two months later (in late July), tillage and ridging operations are carried, along with weeding for maintenance. The same operations are carried again, if necessary, in the late growing season at mid-September (Yonaba et al., 2021). It can be observed on the figure that from 06/09/10 to 07/19/10, 07/30/10 to 08/14/10 and 09/12/10 to 10/05/10, the rate of increase in runoff is low because of the tillage operation, then increases after a cumulative rainfall of 80-100 mm is recorded (Mounirou, 2012).

It appears that on cultivated soils, the observed runoff for each rainfall event is highly dependent on the soil surface conditions than rainfall amount or intensity. Immediately after tillage operation, observed runoff is significantly reduced. Yet, after a cumulative rainfall amount of 80-100 mm falling after the tillage operation has been carried, observed runoff increases significantly.

This significant increase in runoff after the threshold of 80-100 mm of cumulative rainfall can be explained by the regeneration of a structural crust at the soil surface, which further increases runoff (hence limiting infiltration). However, after any tillage operation, this crust is dismantled because of the ploughing. Similar findings have been reported in previous studies, however in the with slightly lower thresholds of 80 mm and 60 mm respectively in the Sahel region (Peugeot et al., 1997; Rockström and Valentin, 1997).

The higher variability observed in runoff coefficients on agricultural soils can be partly explained by the variability in runoff response induced by tillage management operations. Similar results have been reported in previous studies (Cammeraat, 2004; Mathys et al., 2005). These authors further emphasized that the location of runoff measurement strongly influences the observations since runoff, as a process, is largely influenced by the spatial variation of the soil infiltration capacity (texture, structural stability), the microtopography and agricultural practices.

3.3. Analysis of runoff potential (I_1) and effective runoff (I_2) values

Table 7 presents the characteristic values of the kinematic time to equilibrium *Te* and runoff velocity *Vp* distributions, which are key variables in the calculation of the dimensionless numbers I_1 and I_2. Given a scale of observation, *Te* is lower on bare and degraded soils and increases when the runoff length increases. Likewise, given a soil surface condition, the runoff velocity *Vp* increases when the runoff length increases as well. On a plot of 150 m² having a runoff length of 25 m, after the soil imbibition, an average time of 10.6 min on cultivated soils is required for the entire plot to produce surface runoff with an average velocity of 4 $cm.s^{-1}$; Conversely, surface runoff arises on bare and degraded soil in an average time of 6.1 mn, with an average higher velocity of 7.2 $cm.s^{-1}$. In the case of more intense rainfall events, these durations are respectively 6.2 mn (average velocity of 6.8 $cm.s^{-1}$) and 3.4 mn (average velocity of 12.1 $cm.s^{-1}$) on cultivated and bare/degraded soils. At the sub-catchment scale, for which the runoff length is estimated at 541 and 1390 m respectively in BV_1 and BV_2, it takes on average, 16.8 and 27.3 mn (respectively) for the entire area to contribute to runoff production. The average runoff velocities are 56.9 and 88.3 $cm.s^{-1}$ respectively. However, the time to ponding depends on the rainfall intensity and the antecedent soil moisture condition, as also observed by Mounirou, 2012 and Zouré et al., 2019. This time to ponding is lower on bare and degraded soils (which tend to produce runoff quickly) than on cultivated soils. Likewise, in the case of cultivated soils, this time to ponding increases as the area increases.

410 **Table 7.**

411 Characteristic values of *Te* and *Vp* at different scales of observation in Tougou catchment.

Te (mn)	**Cultivated**			**Bare and Degraded**			**Sub-catchment**	
	1 m²	**50 m²**	**150 m²**	**1 m²**	**50 m²**	**150 m²**	**BV1**	**BV2**
Minimum	0.6	2.3	6.2	0.5	1.9	3.4	8.0	16.1
Q1	1.4	5.5	9.7	0.8	2.9	5.2	14.7	24.3
Q2 (Median)	1.6	6.1	10.5	0.9	3.2	5.8	17.0	26.6
Mean	1.6	6.1	10.6	0.9	3.4	6.1	16.8	27.3
Q3	1.7	6.6	11.5	1.0	3.7	6.6	19.3	29.8
Maximum	2.7	10.6	18.6	1.7	6.2	12.6	31.9	43.6
Vp ($cm.s^{-1}$)	**Cultivated**			**Bare and Degraded**			**Sub-catchment**	
	1 m²	**50 m²**	**150 m²**	**1 m²**	**50 m²**	**150 m²**	**BV1**	**BV2**
Minimum	0.6	1.6	2.2	1.0	2.7	3.3	28.2	53.1
Q1	1.0	2.5	3.6	1.6	4.5	6.3	46.6	77.6
Q2 (Median)	1.1	2.7	4.0	1.9	5.2	7.2	53.0	87.1
Mean	1.1	2.8	4.0	1.9	5.2	7.2	56.9	88.3
Q3	1.2	3.0	4.3	2.1	5.8	8.0	61.5	95.3
Maximum	2.7	7.3	6.8	3.1	8.8	12.1	112.7	143.8

412 *Te*: kinematic time to equilibrium. *Vp*: surface runoff velocity. Q1: 1st quartile. Q2: Median. Q3: 3rd quartile.

413 The distribution of the runoff potential index I_1 and the effective runoff index I_2 values,
414 calculated for all the rainfall observations (from 2010 to 2015) is presented in **Fig. 5**. It
415 appears that for cultivated soils, the median (Q2) of the distribution is close to the mean and
416 centred in the boxplot, whereas the whiskers are almost symmetrical. On the other hand, on
417 bare and degraded soils, the median (Q2) is higher than the mean, whereas the distribution is
418 more elongated towards lower values of I_1 and I_2. This is probably because, on bare and
419 degraded soils, even light rainfall events are likely to trigger surface runoff. Mounirou (2012)
420 showed that in Tougou catchment, the preponding rainfall, that is the minimal amount of
421 rainfall to trigger surface runoff is 3.5 mm on bare/degraded soils and 11-13 mm, significantly
422 higher, on cultivated soils, depending on the tillage operation management.

423 Given a spatial scale, the differences in boxplot distributions from one site to another can be
424 attributed to the differences in soil surface hydrodynamical properties and the associated
425 tillage operation management (on cultivated sites). Moreover, it is interesting to consider that
426 at the scale of BV_1 sub-catchment, the value of I_1 and I_2 ranges between 0.44 - 2.90 and 0.08 -
427 0.49 (respectively) in July and August, then between 0.20 - 1.52 and 0.04 - 0.26 (respectively)
428 in September and October. This decrease observed during the rainy season can be explained
429 by the development of vegetation and plant coverage at the soil surface.

Conversely, for bare and degraded soils, given a spatial scale, the values of I_1 and I_2 are relatively low on the DES crust (S6 site) in comparison to the ERO (S4 site) and G (S5 site) crusts whose distributions across sites seem to be almost identical. For the ERO (S4 site) and G (S5 site) crusts, the median is above mean and the distribution is skewed towards lower values. This might be explained with the fact that on bare and degraded soils, lighter rainfall events produce runoff (Mounirou, 2012). At the plot scale, the values of I_1 and I_2 vary between 0.58 - 10.80 and 0.06 - 0.97 (respectively) on ERO (S4 site) and G (S5 site) crusts. Moreover, at the scale of the BV_2 (cultivated) sub-catchment, these values range between 0.70 - 6.63 and 0.10 - 0.75 (respectively). The variation in monthly averages is not significant as the soil surface condition remain almost unchanged throughout the year on bare and degraded soils.

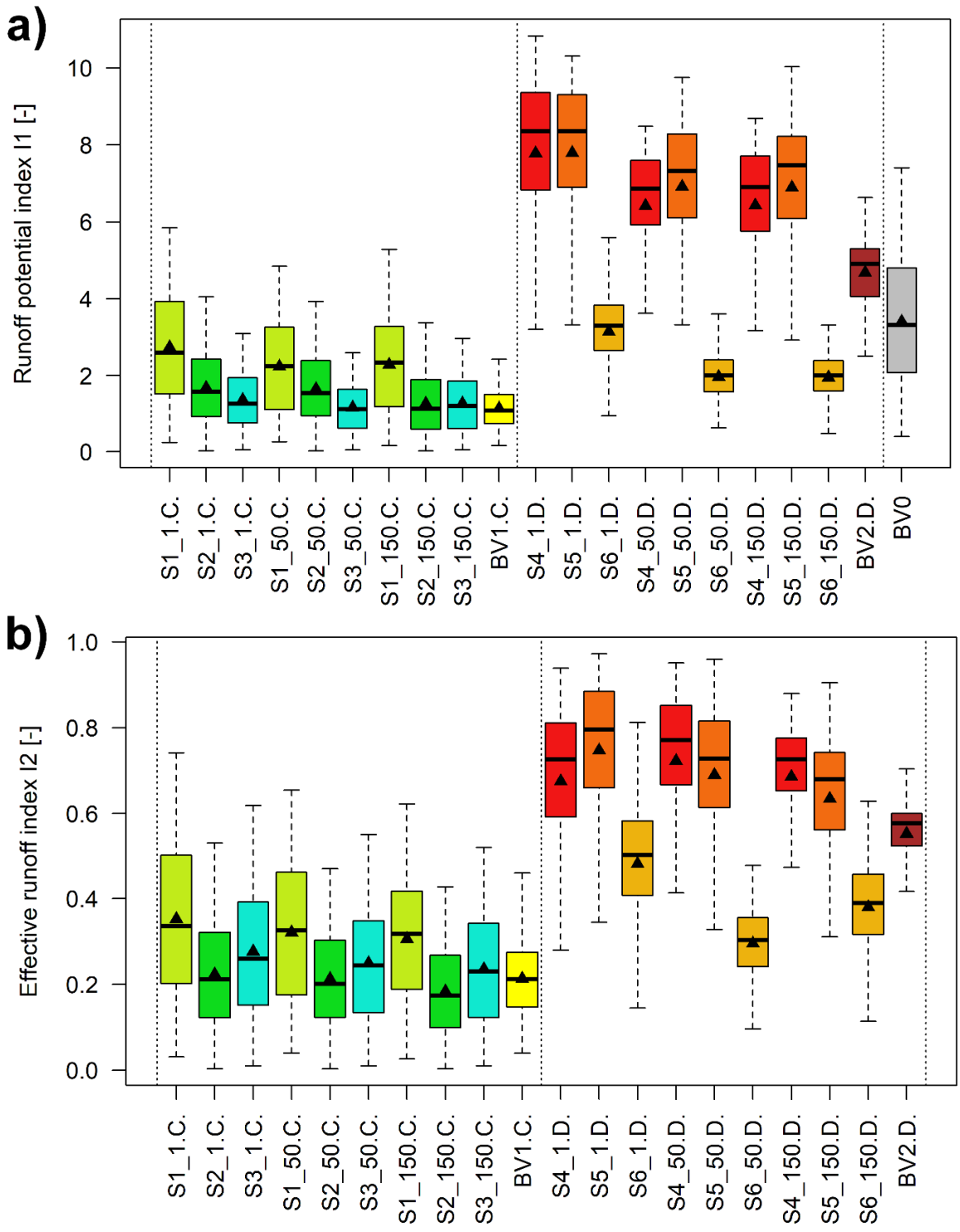

Fig. 5. Distribution of dimensionless indices I_1 and I_2 on measurement sites during the period 2010-2015 in Tougou catchment. a) Values of the runoff potential index I_1. b) Values of the effective runoff index I_2. The boxplots are names using the following convention: "SX" (the site names), followed by the plot size (1 m², 50 m² or 150 m²), followed by the letter C (cultivated) or D (bare or degraded). BV_1 refers to the cultivated sub-catchment and BV_2 to the bare/degraded sub-catchment. BV0 stands for the entire Tougou catchment. The middle bar in the boxplots shows the median (Q2) of the distribution, whereas the black dot triangle shows the mean. In panel b), I_2 is not represented for the entire catchment as it cannot evaluated as defined in this study due to the heterogeneity of soil surface conditions on Tougou watershed.

3.4. Scale size effect on runoff

Fig. 6 shows at different scales of observation (from the plot to the sub-catchment scale) the evolution of the average annual values of the dimensionless indices for both cultivated and degraded uncultivated soils. It appears that for each dimensionless index, there is a significant correlation between the four scales of observation considered in this study (I_1: R^2 = 0.9928 – 0.9970, p-value < 0.001; I_2: R^2 = 0.9837 – 0.9903, p-value < 0.001).Also, it can be observed, as already noted in **section 3.2,** that the spread in the values of the dimensionless indices I_1 and I_2 is lower for degraded and uncultivated soils than in cultivated soils.

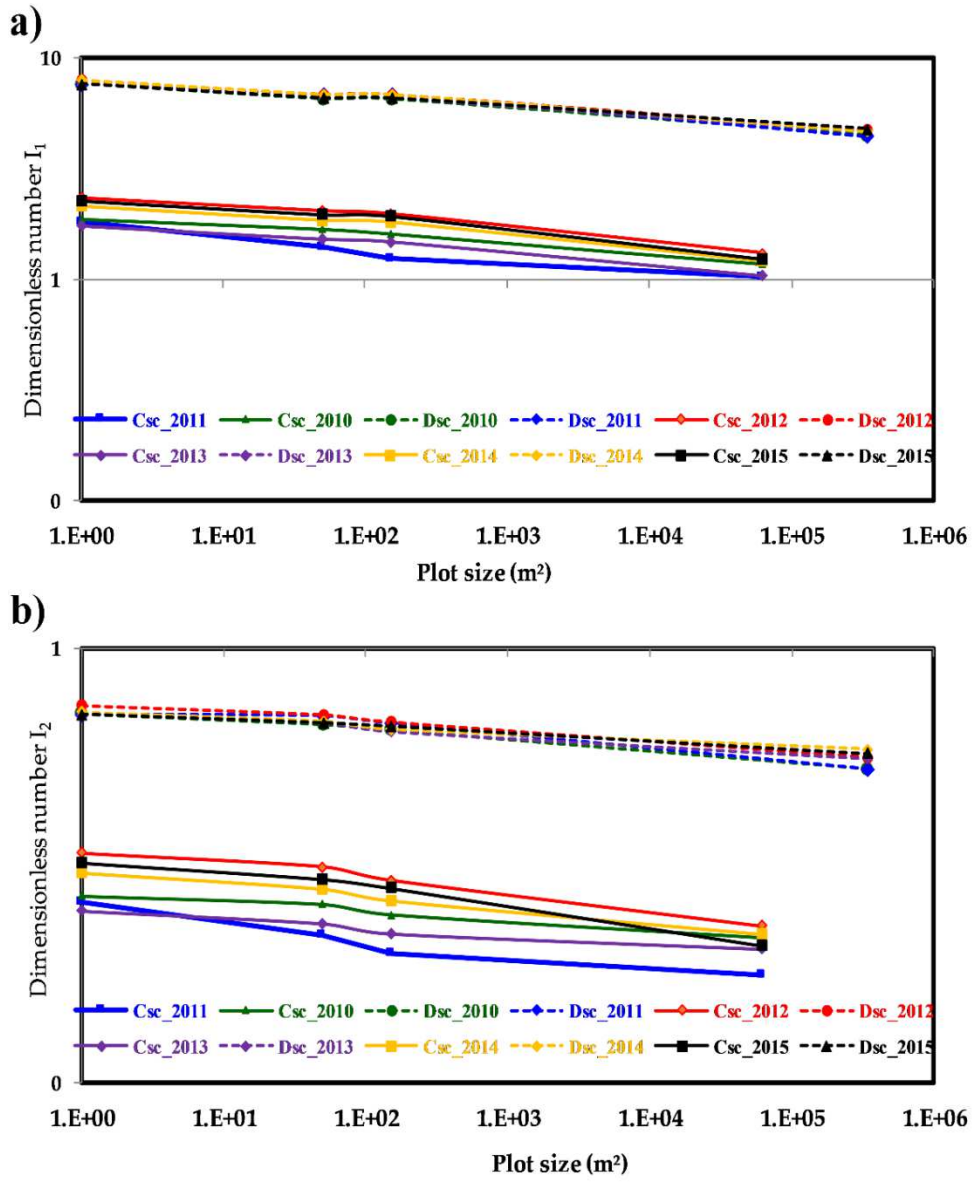

Fig. 6. Evolution of dimensionless indices according to the observation scale size. (a) Relationship between the runoff potential index I_1 and the plot size. (b) Relationship between the effective runoff index I_2 and the plot size. In the two panels above, "*Csc*" refers to "*Cultivated sub-catchment*" whereas "*Dsc*" refers to "*Degraded sub-catchment*". Values of I_1 and I_2 shown in the figure are annual average for each observation scale.

The trend of evolution of each dimensionless index (shown in **Fig. 6**) in relation to the observation scale size is non-linear. The logarithmic decay relationship was found to be providing the best fit ($R^2 > 0.98$ in all cases). **Fig. 7** shows the adjusted scaling law for both dimensionless indices I_1 and I_2.

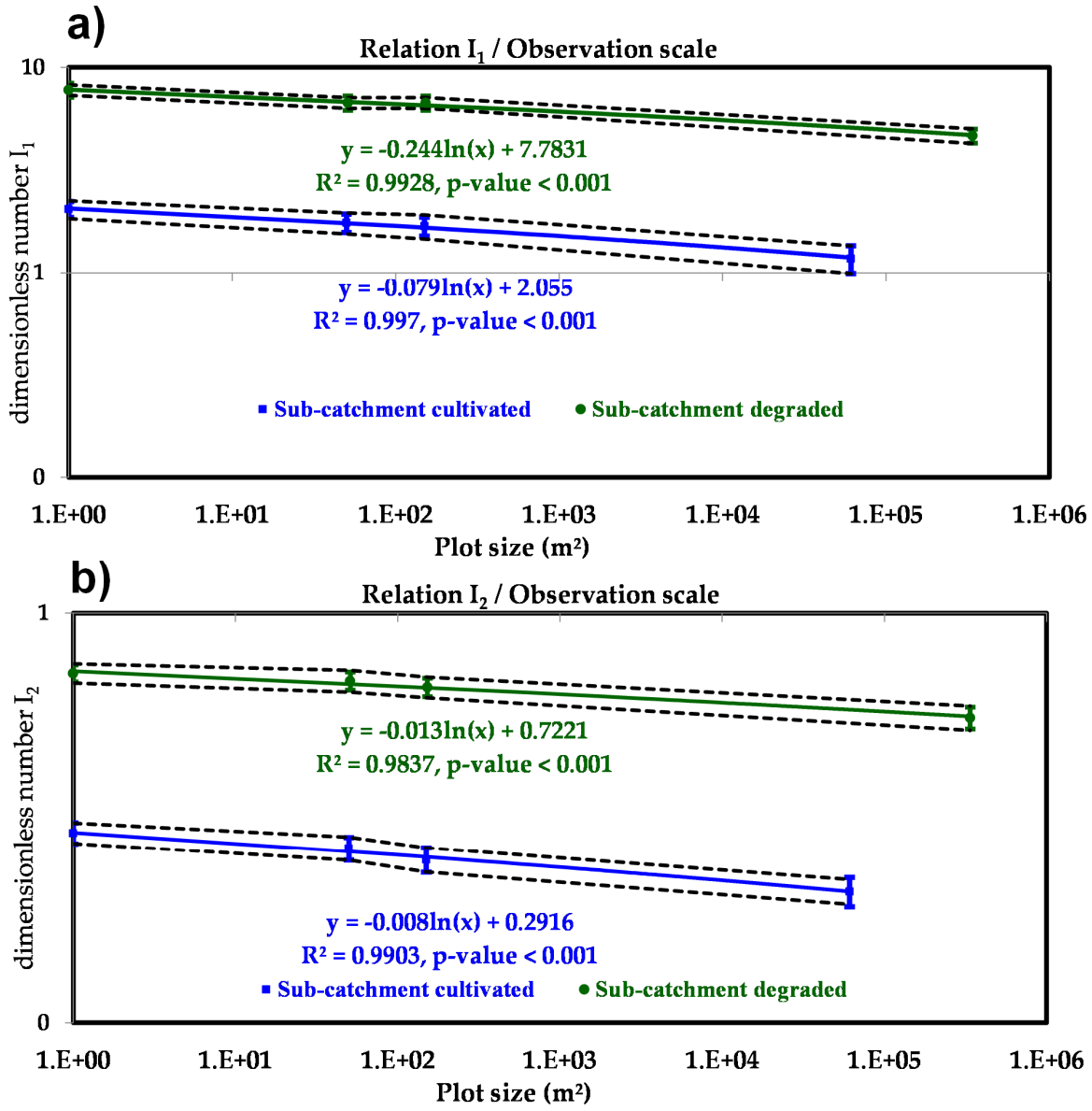

Fig. 7. Logarithmic decay relationship between dimensionless indices and the scales of observation. (a) Relationship between runoff potential index I_1 and the observation scale. (b) Relationship between effective runoff index I_2 and the observation scale. The dotted lines on panels (a) and (b) indicate the width of the 95% confidence interval around the relationships. p-values give the strength of the linear regression with the Spearman non-parametric correlation test (at the 5% level).

4. Discussion

In this study, surface runoff is analysed at various spatial scales (from the unit plot to the catchment) and soil surface conditions to improve our understanding of the effect of the

observation scale on runoff production. First, our results show that surface runoff is significantly higher on bare and degraded soils than on cultivated soils. Also, on both cultivated and bare/degraded soils, surface runoff decreases when the contributing surface area increases, under similar rainfall and antecedent soil moisture conditions. At the plot scale, soil characteristics (microrelief, surface roughness, hydrodynamic parameters) are almost homogeneous and therefore, surface runoff is diffuse. At the sub-catchment and the catchment scales, due to re-infiltration into the hydrographic network and the increased heterogeneity of soil characteristics at such scales, surface runoff is anastomosed and/or concentrated. In this regard, Esteves and Lapetite (2003) showed that the runoff coefficient is significantly non-uniform in space, due to the higher variability of infiltration, surface storage capacity of the soil surface and vegetation development. Such variability occurs both in space and over time and significantly affects runoff. Moreover, these authors showed that at the local scale, infiltration and runoff are almost entirely dependent on the hydraulic properties of the crusts developing at the soil surface. Our results overall are in line with these runoff production mechanisms already reported in the Sahelian context.

To provide a better assessment of the scale effect, two dimensionless indices were defined in this study, based on the main factors of runoff. It is interesting to point out that various runoff indices have been proposed in the literature, mostly based on morphometric characteristics such as the shape, hydrographic network length, drainage density, slope, etc. Some notable examples include the compactness coefficient of Gravelius (1914), the Horton form index (Horton, 1932), the Schumm index (Schumm, 1956), the global slope index (Dubreuil, 1966), the topographic index (Beven, 1997). Such indices have been widely used by hydrologists to quantify the theoretical influence of the catchment morphology on their hydrological response. However, the dimensionless numbers proposed in this study allow us to account for both the catchment morphometric characteristics, but also the rainfall intensity and the soil surface hydrodynamic, which are typically known to be major factors in surface runoff formation especially for Sahelian hydrosystems (Casenave and Valentin, 1992; Karambiri et al., 2003; Zouré et al., 2019; Mounirou et al., 2020).

The runoff potential index I_1 proposed in this study reduces the effect of the slope on the observed runoff. Indeed, it should be acknowledged that the role of slope on runoff is not clearly defined. In a handful of studies (Fox et al., 1997; Chaplot and Le Bissonnais, 2000; Mounirou et al., 2020), an increase in surface runoff with an increase in soil slope is reported. These authors attribute this effect to the decrease in soil surface storage and the decrease of

509 the ponds. As the slope increases, the running water head at the soil surface generally
510 decreases whereas its velocity increases. However, on cultivated plots, due to the weeding
511 operation management, the influence of the slope is moderate since the soil surface roughness
512 and the microtopography is increased. Microtopography plays a key role in surface runoff
513 production primarily through friction, surface storage and spatial distribution of runoff.
514 Kamphorst et al. (2000) showed that an increase in the soil surface roughness causes an
515 increase in friction, which will cause in turn the water head to increase and runoff velocity to
516 decrease, as expressed in the Manning overland flow equation (Manning, 1891). On the other
517 hand, on bare and degraded plots, the absence of ploughing leaves the soil surface roughness
518 and the microtopography untouched. Therefore, the hydraulic slope increases with the
519 topographic slope. On such soil surface conditions, the slope becomes a prominent factor in
520 the surface runoff production as it affects straight the transfer time and therefore the runoff
521 volume.

522 Conversely, some authors showed that there is a threshold above which the slope effect is
523 shadowed by other processes. For example, Janeau et al. (2003) and Ribolzi et al. (2011)
524 observed a decrease in runoff coefficient on tropical cultivated soils in Thailand and Laos,
525 with slopes ranging from 16 to 63%, without rills, gullies or crust development. Moreover,
526 these authors reported the greater compaction of the soil surface on less steep slopes, which
527 was partly explained by the significant decrease in the rainfall kinetic energy on the sloping
528 plot. They argue that the horizontal component of the rainfall kinetic energy, which is more
529 important for steep slopes is transformed into shear, which would limit soil compaction for
530 steep slopes and thereby sustain a stronger infiltration. Overall, it appears that the effect of the
531 slope remains difficult to predict and seems to be strongly dependent on the soil surface
532 conditions.

533 The effective runoff index I_2 proposed in this study reduces the combined effect of rainfall
534 intensity and soil surface hydrodynamic properties (saturated hydraulic conductivity, soil
535 surface roughness, runoff length) on surface runoff observations. Several studies have
536 demonstrated the influence of soil surface conditions on the spatial variability of surface
537 runoff (Moreno et al., 2009; Anache et al., 2017; Langhans et al., 2019). It is also
538 acknowledged that at the local scale, surface runoff is governed by physical laws involving
539 surface roughness, slope and rainfall intensity (Karambiri et al., 2003; Mounirou et al., 2012,
540 2020). Besides, Sivapalan and Wood (1986) showed that at the beginning of a rainfall event,
541 surface runoff is majorly defined by the soil properties, which is typical of arid and semi-arid

Sahelian landscapes. More precisely, as a rainfall event begins, the rainfall intensity is generally lower than soil infiltration capacity, and surface runoff later appears when the infiltrated amount equals the precipitation amount. At this time, the rainfall intensity also equals the soil infiltration capacity. Hence, our effective runoff index I_2 makes it possible to account for the initial losses due to infiltration and storage in micro-ponds at the soil surface.

The use of dimensionless numbers to assess hydrological similarity has already been investigated. Larsen et al. (1994) explained the variability of the runoff coefficient through a dimensionless index defined by the rainfall intensity and the soil characteristics. Similarly, Lyon and Troch (2010) developed a similarity parameter called the "*Péclet index*" to describe the groundwater response in small catchments. Compared to classical morphometric indices, our approach considers both the rainfall intensity, the hydrodynamic properties of soils (saturated hydraulic conductivity, surface roughness, slope, runoff length) which are known to be the main factors affecting surface runoff in typical Sahelian landscapes. It should be noted that the global scale, reflecting the combination of all local interactions, effective or not, very often hides effects of these smaller functional units. Hence, the use of such dimensionless numbers helps in reduce the differences observed at various measurement scales and therefore constitutes an attempt at normalizing such measurements across scales.

Also, it should be highlighted that our results highlight the non-linear nature of runoff as a result of separate contributions and interaction from factors such as spatial heterogeneity of soil hydrodynamic parameters. The scaling relationships proposed in this study are in line with previous research, which reported logarithmic decay relationship to be effective at fitting and describing physical processes such as surface runoff (Woods and Sivapalan, 1997; Labat et al., 2002; Mayor et al., 2011; Ayalew et al., 2014). Our results might also provide useful insight for parameterizing spatial variability of runoff coefficient in distributed hydrologic models (Gnouma, 2006). However, the dimensionless numbers proposed in this study requires first a physical characterization of the observation scale for which they are evaluated (area, runoff length, soil surface conditions, slope, soil surface roughness, saturated hydraulic conductivity). Also, the use of these numbers should be limited to mild slopes (0 to 3%). Moreover, the development of these dimensionless numbers on homogeneous hydrological units prevents their use on catchments with heterogeneous soil surface conditions. In such cases, additional processes such as water storage in ponds emerge as the observation scale increases (Cammeraat, 2004; Lesschen et al., 2009) and such effects are not well accounted in their actual formulations by the dimensionless indices proposed in this study. However, this

study shed light on the groundwork for the future development of surface runoff similarity indices which could later be improved in further research to account for spatial heterogeneity at larger scales.

5. Conclusions

The results in this study illustrate the complexity of hydrological processes and the number of factors involved in the production of runoff. Data collected from representative plots showed that infiltration is low on areas with permanent crusting (bare soil, degraded and uncultivated) and runoff amounts to more than 50% of the annual rainfall. On cultivated soil, however, runoff is less than 25% of the annual rainfall. These results also support that the location of plots on a slope strongly influences the observations. As such, the relative position of the investigated surface is of great importance in the typical Sahelian and semi-arid environment.

This study aimed at assessing how surface runoff evolves from the unit to the catchment scale in a typical Sahelian landscape, under semi-arid climate. Surface runoff was quantified at different spatial scales and on various soil surface conditions in the Tougou catchment. Through monitoring data collected from 2010 to 2015, hydrological similarity relationships at different observation scales were developed based on two dimensionless indices: a runoff potential index I_1 and an effective runoff index I_2. These indices made it possible to reduce the scale effect and to identify functional relationships between the different scales of observation.

Beyond the results presented, the originality of this work lies first in the multi-scale analysis of hydrological processes, and second, in the search for similarity relations between different scales of observation through dimensional analysis. The dimensionless variables defined in this study are primarily designed to assess the hydrologic similarity in a homogeneous catchment at different spatial scales, albeit their use should be considered limited to small Sahelian catchments with mild slopes (0-3%). The dimensionless indices presented in this paper allowed characterization of runoff regardless of the spatial dimension at which it was observed. This is particularly useful in an attempt to extrapolate measurements carried at small scales to broader scales. Furthermore, a key challenge is to develop a methodology for the application of these dimensionless indices in heterogeneous landscapes.

Data availability

All the data used during the study are available upon request from the corresponding author.

Acknowledgements

The authors wish to thank the International Institute for Water and Environmental Engineering (2iE) at Ouagadougou (Burkina Faso) and the laboratory of HydroSciences at Montpellier (France) for their support in completing this research.

Funding

This research did not receive any specific grant from funding agencies in the public, commercial, or not-for-profit sectors.

Appendix A

Theoretical basis and development of dimensionless runoff indices I_1 and I_2

In this appendix, the theoretical basis and assumptions which led to the development of the dimensionless indices proposed in this study is presented. These dimensionless numbers are developed to reduce the effect of the size of the observation scale on runoff observations, hence providing a basis to compare the respective contribution of different factors of runoff production across different scales.

The dimensionless indices proposed in this study are developed considering the topography, surface roughness, saturated hydraulic conductivity, rainfall amount and intensity and antecedent soil moisture (through the antecedent precipitation index and the runoff response time). Although the intensity and the rainfall amount may vary in space and time, simplifying assumptions are made in this study to consider only their average values. The theoretical basis and mathematical development leading to the expression of these dimensionless indexes detailed in this appendix. Relevant symbols and notations used in further equations are presented in **Table A.1**.

Table A.1.

Symbols and notations used in this appendix.

Symbol	Unit	Description
K	mm.h^{-1}	*Unsaturated soil hydraulic conductivity. As time increases, K tends towards the saturated soil hydraulic conductivity.*
i	mm.h^{-1}	*Instantaneous rainfall intensity at a given time t.*
i_m	mm.h^{-1}	*Average rainfall intensity.*
S_0	-	*Plot slope.*
x	m	*Distance downstream measured from the plot origin.*
L	m	*Total plot length, corresponding to the total flow length.*
n	s.m$^{-1/3}$	*Manning roughness of the plot soil surface.*
h	m	*Overland runoff depth at abscissa x.*
T	s	*Time.*
T_e	s	*Equilibrium time. It is the time at which all the plot surface is contributing to the observed runoff.*
v	m.s^{-1}	*Instantaneous overland flow velocity at abscissa x on the plot (v = dx/dt).*

Hydraulic engineers, in the late 1800s, were interested in developing rational formulations for open channel flow. The most common formula, to date, is that of Manning-Strickler which assumes that the flow is uniform, that is to say the pressure drop is due to the slope of the channel S_0 and the hydraulic radius R_h, as shown in **Equation A.1** (Chanson, 2004):

$$v = \frac{\sqrt{S_0}\, R_H^{2/3}}{n} \tag{A.1}$$

where v *(m.s^{-1})* is the flow velocity, S_0 is the channel slope, R_H *(m)* the hydraulic radius and n *(s.m$^{-1/3}$)* the Manning roughness coefficient. This formula relates the flow velocity to the square root of the channel slope S_0. As such, one can identify two runoff governing parameters: the slope and the roughness or soil surface condition (in case of overland flow).

If we assume a very large cross-section flow and also assume this cross section is of rectangular form shape, where the flow depth h is very small as compared to the flow width b, the hydraulic radius is further reduced to the flow height, as shown in **Equation A.2**:

$$R_H = \frac{b\,h}{b + 2\,h} \cong h \tag{A.2}$$

where b *(m)* is the flow width and h *(m)* is the flow depth. This hypothesis simplifies **Equation A.1** which is now reduced to the form shown in **Equation A.3**:

$$v = \frac{\sqrt{S_0}\, h^{2/3}}{n} \tag{A.3}$$

Let us consider an experimental plot case under a specific rainfall event illustrated in **Fig. A.1**.

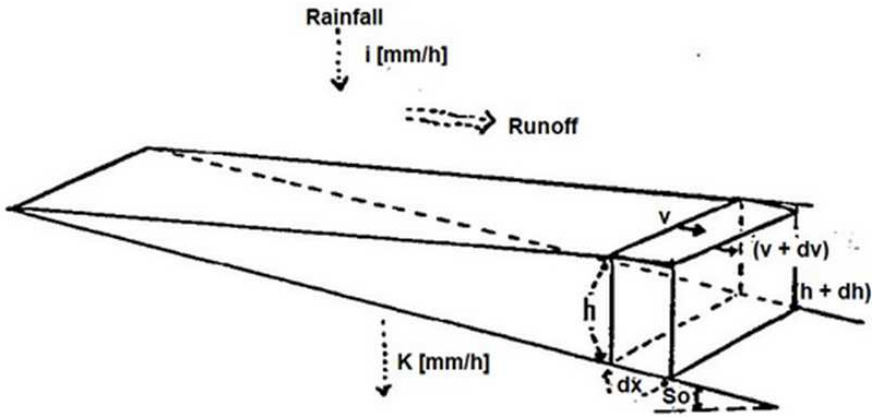

Fig. A.1. Conceptual representation of a rainfall event occurring on a plot and triggering surface runoff. Adapted from Guillobez (1990).

At a given time *t* after the onset of a rainfall event, at a distance *x* from the upstream plot origin, the instantaneous runoff height observed is *h*, flowing at velocity *v*. After a small amount of time increment *dt*, the cross-section of water has moved by a small increment in distance *dx*. The velocity has increased by *dv* and is now *v* + *dv*. The water height, because of the rainfall input received and the losses by infiltration along the flow path travelled *dx*, has now a height of *h* + *dh*. The continuity equation (mass conservation), yields **Equation A.4**:

$$(v + dv)\,(h + dh) = v\,h + (i - K)\,dx \tag{A.4}$$

Neglecting second order product term (*dh x dv)*, **Equation A.4** is further reduced to **Equation A.5**:

$$h\,dv + v\,dh = (i - K)\,dx \;\rightarrow\; d(h\,v) = (i - K)\,dx \tag{A.5}$$

Based on **Equation A.3**, **Equation A.5**can be rewritten as follows (**Equations A.6-A.8**):

$$h = \left(\frac{n\,v}{\sqrt{S_0}}\right)^{3/2} \rightarrow \quad d\left[v\left(\frac{n\,v}{\sqrt{S_0}}\right)^{3/2}\right] = (i - K)\,dx \tag{A.6}$$

$$\left(\frac{n}{\sqrt{S_0}}\right)^{3/2} d\left[v^{5/2}\right] = (i - K)\,dx \tag{A.7}$$

$$\frac{5}{2}\left(\frac{n}{\sqrt{S_0}}\right)^{3/2} v^{3/2}\, dv = (i-K)\, dx \tag{A.8}$$

Dividing both left-hand and right-hand terms by *dt* and replacing velocity *v* by *dx/dt*, **Equation A.8** is further rewritten as **Equation A.9**:

$$\frac{5}{2}\left(\frac{n}{\sqrt{S_0}}\right)^{3/2} \left(\frac{dx}{dt}\right)^{3/2} \frac{d^2x}{dt^2} = (i-K)\, \frac{dx}{dt} \tag{A.9}$$

Simplifying **Equation A.9** by *dx/dt* brings the differential equation shown in **Equation A.10**:

$$\frac{5}{2}\left(\frac{n}{\sqrt{S_0}}\right)^{3/2} \left(\frac{dx}{dt}\right)^{1/2} \frac{d^2x}{dt^2} = (i-K) \tag{A.10}$$

Further, by noticing the equivalence shown in **Equation A.11**:

$$\left(\frac{dx}{dt}\right)^{1/2} \frac{d^2x}{dt^2} = \frac{2}{3}\frac{d}{dt}\left(\frac{dx}{dt}\right)^{3/2} \tag{A.11}$$

Equation A.10 can now be rewritten into **Equation A.12**:

$$d\left(\frac{dx}{dt}\right)^{3/2} = \frac{3}{5}\left(\frac{\sqrt{S_0}}{n}\right)^{3/2} (i-K)\, dt \tag{A.12}$$

In reality, *i* and *K* varies as a function of time *t*. However, when *t* is large, *i* and *K* tend respectively to the average rainfall intensity (i_m) and the saturated hydraulic conductivity (*Ks*). By integrating **Equation A.12** over time, **Equations A.13** and **A.14** are obtained.

$$\left(\frac{dx}{dt}\right)^{3/2} = \frac{3}{5}\left(\frac{\sqrt{S_0}}{n}\right)^{3/2} \int_0^t (i-K)\, dt = \frac{3}{5}\left(\frac{\sqrt{S_0}}{n}\right)^{3/2} (i_m - K_s)\, t \tag{A.13}$$

$$v = \left(\frac{dx}{dt}\right) = \left({}^{3}/_{5}\right)^{2/3} \frac{\sqrt{S_0}}{n} (i_m - K_s)^{2/3} t^{2/3} \quad \text{(A.14)}$$

665 Integrating **Equation A.14** over time yields **Equation A.15**:

$$x = \left({}^{3}/_{5}\right)^{5/3} \frac{\sqrt{S_0}}{n} (i_m - K_s)^{2/3} t^{5/3} \quad \text{(A.15)}$$

666 **Equation A.14** relates the flow velocity *v* at distance *x* to the time *t*. This velocity is as high
667 as the slope of the plot is steep, or the rainfall duration is long, or the rainfall intensity is high
668 or the roughness is low. **Equation A.15** relates distance *x* to the time *t*. Knowing the dripping
669 length (or the plot length) helps in estimating the equilibrium time *Te* whose value is at
670 minimum equal to the concentration time given by **Equation A.16**:

$$T_e = {}^{5}/_{3} \left(\frac{n\,L}{(i_m - K_s)^{2/3} \sqrt{S_0}} \right)^{3/5} \quad \text{(A.16)}$$

671 The term *Te* in **Equation A.16** can be rewritten as given by **Equation A.17** (also **Equation 6**
672 in this paper, Julien and Moglen, 1990):

$$T_e = \beta \left(\frac{L}{\alpha \times i^{\beta - 1}} \right)^{1/\beta} \quad \text{(A.17)}$$

673 where *L (m)* is the plot length, $i = i_m - K_S$ is the infiltration excess, α and β are parameters.
674 Combining Manning resistance turbulent flow equation with a kinematic wave approximation
675 yields β = *5/3* (Julien and Moglen, 1990). Parameter α, on the other hand, is given by
676 **Equation A.18** (also **Equation 7** in this paper):

$$\alpha = \frac{1}{n} \times \sqrt{S_0} \quad \text{(A.18)}$$

677 where S_0 is the plot slope and *n* $[s.m^{-1/3}]$ is the Manning roughness coefficient.

678 Concentration time is therefore as high as the slope is mild, the rainfall intensity is low and
679 the soil surface is rough. It also increases as the plot length increases. It can therefore be

concluded that the overland flow velocity at distance *x*, also called *runoff intensity*, is a function of the four following parameters:

- the relative rainfall intensity, also called *excess precipitation*,
- the soil surface roughness,
- the slope of the plot,
- the rainfall event duration.

In this article, we sought to reduce these flow-related variables to two dimensionless numbers to reduce the effect of the size of the observation plot. Although the intensity and the rainfall amount vary in both space and time, simplifying assumptions have been made to consider only the average values. The two dimensionless indexes I_1 and I_2 are therefore defined as follows:

(i) the runoff potential index $\boldsymbol{I_1}$ which is the ratio of the runoff coefficient of the plot to the square root of its slope. It expresses the potential for runoff from the plot while reducing the effect of microrelief (explicitly the slope) on runoff production. Its formulation is given in **Equation 4** (in the paper).

$$I_1 = \frac{K_r}{\sqrt{S_0}} \qquad (\mathbf{4})$$

(ii) the dimensionless number I_2 which is the ratio of the depth of overland flow *R (mm)* measured at a given observation scale to the term (*P - Ks x Te*) where *P (mm)* is the rainfall amount, *Ks* ($mm.h^{-1}$) the saturated hydraulic conductivity and *Te (h)* the equilibrium time. I_2 is given in **Equation 5** (in the paper).

$$I_2 = \frac{R}{P - K_s \times T_e} \qquad (\mathbf{5})$$

References

Albergel, J., 1987. Sécheresse, désertification et ressources en eau de surface : application aux petits bassins du Burkina Faso, in: The influence of climate change and climatic variability on the hydrologic regime and water resources. pp. 355–365.

Anache, J.A.A., Wendland, E.C., Oliveira, P.T.S., Flanagan, D.C., Nearing, M.A., 2017. Runoff and soil erosion plot-scale studies under natural rainfall: A meta-analysis of the Brazilian experience. CATENA 152, 29–39. https://doi.org/10.1016/j.catena.2017.01.003

Anderson, J.R., Hardy, E.E., Roach, J.T., Witmer, R.E., 1976. A land use and land cover classification system for use with remote sensor data (Professional Paper), Professional Paper.

Antoine, M., Javaux, M., Bielders, C.L., 2011. Integrating subgrid connectivity properties of the micro-topography in distributed runoff models, at the interrill scale. Journal of Hydrology 403, 213–223. https://doi.org/10.1016/j.jhydrol.2011.03.027

Ayalew, T.B., Krajewski, W.F., Mantilla, R., 2014. Connecting the power-law scaling structure of peak-discharges to spatially variable rainfall and catchment physical properties. Advances in Water Resources 71, 32–43. https://doi.org/10.1016/j.advwatres.2014.05.009

Barbier, B., Yacouba, H., Karambiri, H., Zoromé, M., Somé, B., 2009. Human vulnerability to climate variability in the Sahel: farmers' adaptation strategies in northern Burkina Faso. Environmental Management 43, 790–803. https://doi.org/10.1007/s00267-008-9237-9

Beven, K., 1997. TOPMODEL: a critique. Hydrological processes 11, 1069–1085. https://doi.org/10.1002/(SICI)1099-1085(199707)11:9<1069::AID-HYP545>3.0.CO;2-O

Blöschl, G., Bierkens, M.F.P., Chambel, A., Cudennec, C., Destouni, G., Fiori, A., Kirchner, J.W., McDonnell, J.J., Savenije, H.H.G., Sivapalan, M., Stumpp, C., Toth, E., Volpi, E., Carr, G., Lupton, C., Salinas, J., Széles, B., Viglione, A., Aksoy, H., Allen, S.T., Amin, A., Andréassian, V., Arheimer, B., Aryal, S.K., Baker, V., Bardsley, E., Barendrecht, M.H., Bartosova, A., Batelaan, O., Berghuijs, W.R., Beven, K., Blume, T., Bogaard, T., Borges de Amorim, P., Böttcher, M.E., Boulet, G., Breinl, K., Brilly, M., Brocca, L., Buytaert, W., Castellarin, A., Castelletti, A., Chen, X., Chen, Yangbo, Chen, Yuanfang, Chifflard, P., Claps, P., Clark, M.P., Collins, A.L., Croke, B., Dathe, A., David, P.C., de Barros, F.P.J., de Rooij, G., Di Baldassarre, G., Driscoll, J.M., Duethmann, D., Dwivedi, R., Eris, E., Farmer, W.H., Feiccabrino, J., Ferguson, G., Ferrari, E., Ferraris, S., Fersch, B., Finger, D., Foglia, L., Fowler, K., Gartsman, B., Gascoin, S., Gaume, E., Gelfan, A., Geris, J., Gharari, S., Gleeson, T., Glendell, M., Gonzalez Bevacqua, A., González-Dugo, M.P., Grimaldi, S., Gupta, A.B., Guse, B., Han, D., Hannah, D., Harpold, A., Haun, S., Heal, K., Helfricht, K., Herrnegger, M., Hipsey, M., Hlaváčiková, H., Hohmann, C., Holko, L., Hopkinson, C., Hrachowitz, M., Illangasekare, T.H., Inam, A., Innocente, C., Istanbulluoglu, E., Jarihani, B., Kalantari, Z., Kalvans, A., Khanal, S., Khatami, S., Kiesel, J., Kirkby, M., Knoben, W., Kochanek, K., Kohnová, S., Kolechkina, A., Krause, S., Kreamer, D., Kreibich, H., Kunstmann, H., Lange, H., Liberato, M.L.R., Lindquist, E., Link, T., Liu, J., Loucks, D.P., Luce, C., Mahé, G., Makarieva, O., Malard, J., Mashtayeva, S., Maskey, S., Mas-Pla, J., Mavrova-Guirguinova, M., Mazzoleni, M., Mernild, S., Misstear, B.D., Montanari, A., Müller-Thomy, H., Nabizadeh, A., Nardi, F., Neale, C., Nesterova, N., Nurtaev, B., Odongo, V.O., Panda, S., Pande, S., Pang, Z., Papacharalampous, G., Perrin, C., Pfister, L., Pimentel, R., Polo, M.J., Post, D., Prieto Sierra, C., Ramos, M.-H., Renner, M., Reynolds, J.E., Ridolfi, E., Rigon, R., Riva, M., Robertson, D.E., Rosso, R., Roy, T., Sá, J.H.M., Salvadori, G., Sandells, M., Schaefli, B., Schumann, A., Scolobig, A., Seibert, J., Servat, E., Shafiei, M., Sharma, A., Sidibe, M., Sidle, R.C., Skaugen, T., Smith, H., Spiessl, S.M., Stein, L., Steinsland, I., Strasser, U., Su, B., Szolgay, J., Tarboton, D., Tauro, F., Thirel, G., Tian, F., Tong, R., Tussupova, K., Tyralis, H., Uijlenhoet, R., van Beek, R., van der Ent, R.J., van der Ploeg, M., Van Loon, A.F., van Meerveld, I., van Nooijen, R., van Oel, P.R., Vidal, J.-P., von Freyberg, J., Vorogushyn, S., Wachniew, P., Wade, A.J., Ward, P., Westerberg, I.K., White, C., Wood, E.F., Woods, R., Xu, Z., Yilmaz, K.K., Zhang, Y.,

2019. Twenty-three unsolved problems in hydrology (UPH) – a community perspective. Hydrological Sciences Journal 64, 1141–1158. https://doi.org/10.1080/02626667.2019.1620507

Boix-Fayos, C., Martínez-Mena, M., Calvo-Cases, A., Arnau-Rosalén, E., Albaladejo, J., Castillo, V., 2007. Causes and underlying processes of measurement variability in field erosion plots in Mediterranean conditions. Earth Surface Processes and Landforms 32, 85–101. https://doi.org/10.1002/esp.1382

Cammeraat, E.L.H., 2004. Scale dependent thresholds in hydrological and erosion response of a semi-arid catchment in southeast Spain. Agriculture, Ecosystems & Environment 104, 317–332. https://doi.org/10.1016/j.agee.2004.01.032

Cammeraat, L.H., 2002. A review of two strongly contrasting geomorphological systems within the context of scale. Earth Surface Processes and Landforms 27, 1201–1222. https://doi.org/10.1002/esp.421

Cantón, Y., Solé-Benet, A., de Vente, J., Boix-Fayos, C., Calvo-Cases, A., Asensio, C., Puigdefábregas, J., 2011. A review of runoff generation and soil erosion across scales in semiarid south-eastern Spain. Journal of Arid Environments 75, 1254–1261. https://doi.org/10.1016/j.jaridenv.2011.03.004

Casenave, A., Valentin, C., 1992. A runoff capability classification system based on surface features criteria in semi-arid areas of West Africa. Journal of Hydrology 130, 231–249. https://doi.org/10.1016/0022-1694(92)90112-9

Cerdan, O., Govers, G., Le Bissonnais, Y., Van Oost, K., Poesen, J., Saby, N., Gobin, A., Vacca, A., Quinton, J., Auerswald, K., Klik, A., Kwaad, F.J.P.M., Raclot, D., Ionita, I., Rejman, J., Rousseva, S., Muxart, T., Roxo, M.J., Dostal, T., 2010. Rates and spatial variations of soil erosion in Europe: A study based on erosion plot data. Geomorphology 122, 167–177. https://doi.org/10.1016/j.geomorph.2010.06.011

Cerdan, O., Le Bissonnais, Y., Govers, G., Lecomte, V., van Oost, K., Couturier, A., King, C., Dubreuil, N., 2004. Scale effect on runoff from experimental plots to catchments in agricultural areas in Normandy. Journal of Hydrology 299, 4–14. https://doi.org/10.1016/j.jhydrol.2004.02.017

Chanson, H., 2004. Hydraulics of open channel flow. Elsevier.

Chaplot, V., Le Bissonnais, Y., 2000. Field measurements of interrill erosion under different slopes and plot sizes. Earth Surface Processes and Landforms: The Journal of the British Geomorphological Research Group 25, 145–153. https://doi.org/10.1002/(SICI)1096-9837(200002)25:2<145::AID-ESP51>3.0.CO;2-3

Corradini, C., Morbidelli, R., Melone, F., 1998. On the interaction between infiltration and Hortonian runoff. Journal of Hydrology 204, 52–67. https://doi.org/10.1016/S0022-1694(97)00100-5

Cristiano, E., Veldhuis, M., Wright, D.B., Smith, J.A., Giesen, N., 2019. The Influence of Rainfall and Catchment Critical Scales on Urban Hydrological Response Sensitivity. Water Resources Research 55, 3375–3390. https://doi.org/10.1029/2018WR024143

Dubreuil, P., 1966. Les caractères physiques et morphologiques des bassins versants : leur détermination avec une précision acceptable. Cahiers ORSTOM.Série Hydrologie 3, 13–29.

Dugué, P., Rodriguez, L., Ouoba, B., Sawadogo, I., 1994. Techniques d'amélioration de la production agricole en zone soudano-sahélienne: manuel à l'usage des techniciens du développement rural, élaboré au Yatenga, Burkina Faso. CIRAD-SAR, Montpellier.

Esteves, M., Lapetite, J.M., 2003. A multi-scale approach of runoff generation in a Sahelian gully catchment: a case study in Niger. CATENA 50, 255–271. https://doi.org/10.1016/S0341-8162(02)00136-4

806 Fox, D., Bryan, R., Price, A., 1997. The influence of slope angle on final infiltration rate for
807 interrill conditions. Geoderma 80, 181–194. https://doi.org/10.1016/S0016-
808 7061(97)00075-X
809 Gbohoui, Y.P., Paturel, J.-E., Fowe Tazen, Mounirou, L.A., Yonaba, R., Karambiri, H.,
810 Yacouba, H., 2021. Impacts of climate and environmental changes on water resources:
811 A multi-scale study based on Nakanbé nested watersheds in West African Sahel.
812 Journal of Hydrology: Regional Studies 35, 100828.
813 https://doi.org/10.1016/j.ejrh.2021.100828
814 Gnouma, R., 2006. Aide à la calibration d'un modèle hydrologique distribué au moyen d'une
815 analyse des processus hydrologiques: application au bassin versant de l'Yzeron (PhD
816 Thesis). Institut National des Sciences Appliquées de Lyon.
817 Gomi, T., Sidle, R.C., Miyata, S., Kosugi, K., Onda, Y., 2008. Dynamic runoff connectivity
818 of overland flow on steep forested hillslopes: Scale effects and runoff transfer:
819 DYNAMIC RUNOFF CONNECTIVITY OF OVERLAND FLOW. Water Resources
820 Research 44. https://doi.org/10.1029/2007WR005894
821 Gravelius, H., 1914. Flusskunde, Gravelius, H(arry): Grundriß der gesamten Gewässerkunde.
822 1. G.J. göschen.
823 Gresillon, J.-M., Taha, A., 1998. Les zones saturées contributives en climat méditerranéen:
824 condition d'apparition et influence sur les crues. Hydrological Sciences Journal 43,
825 267–282. https://doi.org/10.1080/02626669809492121
826 Guillobez, S., 1990. Réflexions théoriques du ruissellement et de l'érosion. Bases d'un
827 contrôle, application à la détermination des écartements entre dispositifs anti-érosifs.
828 Bois & Forêts des Tropiques 226, 37–47. https://doi.org/10.19182/bft1990.226.a19654
829 Horton, R.E., 1932. Drainage-basin characteristics. Trans. AGU 13, 350.
830 https://doi.org/10.1029/TR013i001p00350
831 IGB, 2002. Base de données d'Occupation des Terres (BDOT) 2002. Burkina Faso.
832 Janeau, J.-L., Bricquet, J.-P., Planchon, O., Valentin, C., 2003. Soil crusting and infiltration
833 on steep slopes in northern Thailand. European Journal of Soil Science 54, 543–554.
834 https://doi.org/10.1046/j.1365-2389.2003.00494.x
835 Jawuoro, S.O., Koech, O.K., Karuku, G.N., Mbau, J.S., 2017. Effect of piospheres on physio-
836 chemical soil properties in the Southern Rangelands of Kenya. Ecol Process 6, 14.
837 https://doi.org/10.1186/s13717-017-0082-8
838 Jetten, V., de Roo, A., Favis-Mortlock, D., 1999. Evaluation of field-scale and catchment-
839 scale soil erosion models. CATENA 37, 521–541. https://doi.org/10.1016/S0341-
840 8162(99)00037-5
841 Julien, P.Y., Moglen, G.E., 1990. Similarity and length scale for spatially varied overland
842 flow. Water Resources Research 26, 1819–1832.
843 https://doi.org/10.1029/WR026i008p01819
844 Kamphorst, E.C., Jetten, V., Guérif, J., Pitk a ¨ nen, J., Iversen, B.V., Douglas, J.T., Paz, A.,
845 2000. Predicting Depressional Storage from Soil Surface Roughness. Soil Sci. Soc.
846 Am. J. 64, 1749–1758. https://doi.org/10.2136/sssaj2000.6451749x
847 Karambiri, H., Ribolzi, O., Delhoume, J.P., Ducloux, J., Coudrain-Ribstein, A., Casenave, A.,
848 2003. Importance of soil surface characteristics on water erosion in a small grazed
849 Sahelian catchment. Hydrological Processes 17, 1495–1507.
850 https://doi.org/10.1002/hyp.1195
851 Kirkby, M., Bracken, L., Reaney, S., 2002. The influence of land use, soils and topography on
852 the delivery of hillslope runoff to channels in SE Spain. Earth Surface Processes and
853 Landforms 27, 1459–1473. https://doi.org/10.1002/esp.441

Labat, D., Mangin, A., Ababou, R., 2002. Rainfall–runoff relations for karstic springs: multifractal analyses. Journal of Hydrology 256, 176–195. https://doi.org/10.1016/S0022-1694(01)00535-2

Langhans, C., Diels, J., Clymans, W., Van den Putte, A., Govers, G., 2019. Scale effects of runoff generation under reduced and conventional tillage. CATENA 176, 1–13. https://doi.org/10.1016/j.catena.2018.12.031

Larsen, J.E., Sivapalan, M., Coles, N.A., Linnet, P.E., 1994. Similarity analysis of runoff generation processes in real-world catchments. Water Resources Research 30, 1641–1652. https://doi.org/10.1029/94WR00555

Lesschen, J.P., Schoorl, J.M., Cammeraat, L.H., 2009. Modelling runoff and erosion for a semi-arid catchment using a multi-scale approach based on hydrological connectivity. Geomorphology 109, 174–183. https://doi.org/10.1016/j.geomorph.2009.02.030

Lyon, S.W., Troch, P.A., 2010. Development and application of a catchment similarity index for subsurface flow: CATCHMENT SIMILARITY INDEX FOR SUBSURFACE FLOW. Water Resources Research 46. https://doi.org/10.1029/2009WR008500

Manning, R., 1891. On the flow of water in open channels and pipes. Institute of Civil Engineers of Ireland Transactions 20.

Marchal, J.-Y., 1983. Yatenga: nord Haute-Volta: la dynamique d'un espace rural Soudano-Sahélien, Travaux et Documents de l'ORSTOM. ORSTOM.

Mathon, V., Laurent, H., Lebel, T., 2002. Mesoscale convective system rainfall in the Sahel. Journal of applied meteorology 41, 1081–1092. https://doi.org/10.1175/1520-0450(2002)041<1081:MCSRIT>2.0.CO;2

Mathys, N., Klotz, S., Esteves, M., Descroix, L., Lapetite, J.M., 2005. Runoff and erosion in the Black Marls of the French Alps: Observations and measurements at the plot scale. CATENA 63, 261–281. https://doi.org/10.1016/j.catena.2005.06.010

Mayerhofer, C., Meißl, G., Klebinder, K., Kohl, B., Markart, G., 2017. Comparison of the results of a small-plot and a large-plot rainfall simulator – Effects of land use and land cover on surface runoff in Alpine catchments. CATENA 156, 184–196. https://doi.org/10.1016/j.catena.2017.04.009

Mayor, Á.G., Bautista, S., Bellot, J., 2011. Scale-dependent variation in runoff and sediment yield in a semiarid Mediterranean catchment. Journal of Hydrology 397, 128–135. https://doi.org/10.1016/j.jhydrol.2010.11.039

Miyata, S., Gomi, T., Sidle, R.C., Hiraoka, M., Onda, Y., Yamamoto, K., Nonoda, T., 2019. Assessing spatially distributed infiltration capacity to evaluate storm runoff in forested catchments: Implications for hydrological connectivity. Science of The Total Environment 669, 148–159. https://doi.org/10.1016/j.scitotenv.2019.02.453

Mohamadi, M.A., Kavian, A., 2015. Effects of rainfall patterns on runoff and soil erosion in field plots. International Soil and Water Conservation Research 3, 273–281. https://doi.org/10.1016/j.iswcr.2015.10.001

Moreno, N., Wang, F., Marceau, D.J., 2009. Implementation of a dynamic neighborhood in a land-use vector-based cellular automata model. Computers, Environment and Urban Systems 33, 44–54. https://doi.org/10.1016/j.compenvurbsys.2008.09.008

Mounirou, L.A., 2012. Etude du ruissellement et de l'érosion à différentes échelles spatiales sur le bassin versant de Tougou en zone sahélienne du Burkina Faso: quantification et transposition des données (Thèse de Doctorat). Montpellier 2.

Mounirou, L.A., Yacouba, H., Karambiri, H., Paturel, J.-E., Mahé, G., 2012. Measuring runoff by plots at different scales: Understanding and analysing the sources of variation. Comptes Rendus Geoscience 344, 441–448. https://doi.org/10.1016/j.crte.2012.08.004

Mounirou, L.A., Zouré, C.O., Yonaba, R., Paturel, J.-E., Mahé, G., Niang, D., Yacouba, H., Karambiri, H., 2020. Multi-scale analysis of runoff from a statistical perspective in a small Sahelian catchment under semi-arid climate. Arabian Journal of Geosciences 13. https://doi.org/10.1007/s12517-020-5141-2

Nyamekye, C., Thiel, M., Schönbrodt-Stitt, S., Zoungrana, B., Amekudzi, L., 2018. Soil and Water Conservation in Burkina Faso, West Africa. Sustainability 10, 3182. https://doi.org/10.3390/su10093182

Peters-Lidard, C.D., Clark, M., Samaniego, L., Verhoest, N.E.C., van Emmerik, T., Uijlenhoet, R., Achieng, K., Franz, T.E., Woods, R., 2017. Scaling, Similarity, and the Fourth Paradigm for Hydrology (preprint). Catchment hydrology/Modelling approaches. https://doi.org/10.5194/hess-2016-695

Peugeot, C., Esteves, M., Galle, S., Rajot, J.L., Vandervaere, J.P., 1997. Runoff generation processes: results and analysis of field data collected at the East Central Supersite of the HAPEX-Sahel experiment. Journal of Hydrology 188–189, 179–202. https://doi.org/10.1016/S0022-1694(96)03159-9

Puech, C., DARTUS, D., Bailly, J., Estupina-Borrell, V., 2003. Hydrologie distribuée, télédétection et problèmes d'échelle. Bulletin-Société française de photogrammétrie et de télédétection 11–21.

Reaney, S.M., Bracken, L.J., Kirkby, M.J., 2007. Use of the Connectivity of Runoff Model (CRUM) to investigate the influence of storm characteristics on runoff generation and connectivity in semi-arid areas. Hydrological Processes 21, 894–906. https://doi.org/10.1002/hyp.6281

Reynolds, W., Topp, C., 2008. Soil Water Analyses: Principles and Parameters, in: Carter, M.R., Gregorich, E.G. (Eds.), Soil Sampling and Methods of Analysis. Canadian Society of Soil Science ; CRC Press, [Pinawa, Manitoba] : Boca Raton, FL.

Ribolzi, O., Patin, J., Bresson, L.-M., Latsachack, K., Mouche, E., Sengtaheuanghoung, O., Silvera, N., Thiébaux, J.-P., Valentin, C., 2011. Impact of slope gradient on soil surface features and infiltration on steep slopes in northern Laos. Geomorphology 127, 53–63. https://doi.org/10.1016/j.geomorph.2010.12.004

Rockström, J., Valentin, C., 1997. Hillslope dynamics of on-farm generation of surface water flows: The case of rain-fed cultivation of pearl millet on sandy soil in the Sahel. Agricultural Water Management 33, 183–210. https://doi.org/10.1016/S0378-3774(96)01282-6

Sawadogo, H., Zombre, N.P., Bock, L., Lacroix, D., 2008. Evolution de l'occupation du sol de Ziga dans le Yatenga (Burkina Faso) à partir de photographies aériennes. Télédétection 8, 59–73.

Sawicz, K., Wagener, T., Sivapalan, M., Troch, P.A., Carrillo, G., 2011. Catchment classification: empirical analysis of hydrologic similarity based on catchment function in the eastern USA. Hydrology and Earth System Sciences 15, 2895–2911. https://doi.org/10.5194/hess-15-2895-2011

Schumm, S.A., 1956. Evolution of drainage systems and slopes in badlands at Perth Amboy, New Jersey. Geological society of America bulletin 67, 597–646. https://doi.org/10.1130/0016-7606(1956)67[597:EODSAS]2.0.CO;2

Sivapalan, M., Beven, K., Wood, E.F., 1987. On hydrologic similarity: 2. A scaled model of storm runoff production. Water Resour. Res. 23, 2266–2278. https://doi.org/10.1029/WR023i012p02266

Sivapalan, M., Jothityangkoon, C., Menabde, M., 2002. Linearity and nonlinearity of basin response as a function of scale: Discussion of alternative definitions: Technical Note. Water Resources Research 38, 4-1-4–5. https://doi.org/10.1029/2001WR000482

952 Sivapalan, M., Kalma, J.D., 1995. Scale problems in hydrology: Contributions of the
953 robertson workshop. Hydrological Processes 9, 243–250.
954 https://doi.org/10.1002/hyp.3360090304
955 Sivapalan, M., Wood, E.F., 1986. Spatial Heterogeneity and Scale in the Infiltration Response
956 of Catchments, in: Gupta, V.K., Rodríguez-Iturbe, I., Wood, E.F. (Eds.), Scale
957 Problems in Hydrology. Springer Netherlands, Dordrecht, pp. 81–106.
958 Stomph, T.J., de Ridder, N., Steenhuis, T.S., Van de Giesen, N.C., 2002. Scale effects of
959 Hortonian overland flow and rainfall-runoff dynamics: laboratory validation of a
960 process-based model. Earth Surface Processes and Landforms 27, 847–855.
961 https://doi.org/10.1002/esp.356
962 Tatard, L., Planchon, O., Wainwright, J., Nord, G., Favis-Mortlock, D., Silvera, N., Ribolzi,
963 O., Esteves, M., Huang, C.H., 2008. Measurement and modelling of high-resolution
964 flow-velocity data under simulated rainfall on a low-slope sandy soil. Journal of
965 Hydrology 348, 1–12. https://doi.org/10.1016/j.jhydrol.2007.07.016
966 Tillotson, P.M., Nielsen, D.R., 1984. Scale factors in soil science : Dimensional analysis,
967 inspectional analysis, functional normalization, similitude analysis. Journal of the Soil
968 Science Society of America (USA).
969 Van de Giesen, N., Stomph, T.-J., Ajayi, A.E., Bagayoko, F., 2011. Scale effects in Hortonian
970 surface runoff on agricultural slopes in West Africa: Field data and models.
971 Agriculture, Ecosystems & Environment 142, 95–101.
972 https://doi.org/10.1016/j.agee.2010.06.006
973 Van de Giesen, N., Stomph, T.J., de Ridder, N., 2005. Surface runoff scale effects in West
974 African watersheds: modeling and management options. Agricultural Water
975 Management 72, 109–130. https://doi.org/10.1016/j.agwat.2004.09.007
976 Wagener, T., Sivapalan, M., Troch, P., Woods, R., 2007. Catchment Classification and
977 Hydrologic Similarity. Geography Compass 1, 901–931.
978 https://doi.org/10.1111/j.1749-8198.2007.00039.x
979 Woods, R.A., Sivapalan, M., 1997. A connection between topographically driven runoff
980 generation and channel network structure. Water Resources Research 33, 2939–2950.
981 https://doi.org/10.1029/97WR01880
982 Yonaba, Roland, Biaou, A.C., Koïta, M., Tazen, F., Mounirou, L.A., Zouré, C.O., Queloz, P.,
983 Karambiri, H., Yacouba, H., 2021. A dynamic land use/land cover input helps in
984 picturing the Sahelian paradox: Assessing variability and attribution of changes in
985 surface runoff in a Sahelian watershed. Science of The Total Environment 757,
986 143792. https://doi.org/10.1016/j.scitotenv.2020.143792
987 Yonaba, R., Koïta, M., Mounirou, L.A., Tazen, F., Queloz, P., Biaou, A.C., Niang, D., Zouré,
988 C., Karambiri, H., Yacouba, H., 2021. Spatial and transient modelling of land use/land
989 cover (LULC) dynamics in a Sahelian landscape under semi-arid climate in northern
990 Burkina Faso. Land Use Policy 103, 105305.
991 https://doi.org/10.1016/j.landusepol.2021.105305
992 Zouré, C., 2019. Etude des performances hydrologiques des techniques culturales dans un
993 contexte de changement climatique en zone sahélienne du Burkina Faso (PhD Thesis).
994 https://doi.org/10.13140/RG.2.2.12144.20480
995 Zouré, C., Queloz, P., Koïta, M., Niang, D., Fowé, T., Yonaba, R., Consuegra, D., Yacouba,
996 H., Karambiri, H., 2019. Modelling the water balance on farming practices at plot
997 scale: Case study of Tougou watershed in Northern Burkina Faso. Catena 173, 59–70.
998 https://doi.org/10.1016/j.catena.2018.10.002